Flavor Tagging at KEK B-factory

Koji Hara
High Energy Physics Group
Department of Physics at Osaka University

March 1, 2000

Acknowledgment

First, I would like to thank my advisor, Prof. Yorikiyo Nagashima, for giving me a chance to work on a research in high energy physics.

I would like to express my special thanks to Dr. Masashi Hazumi. Without his precious advise and discussion with him, this thesis work wouldn't have finished.

I am deeply thankful to Prof. A. Maki, Prof. T. Yamanaka, Dr. M. Takita, Dr. T. Hara, Dr. K. Trabelsi for answering many of my silly and boring questions on high energy physics experiment. I am specially thankful to Dr. D. Jackson for careful check for the manuscript.

My thanks go to all the members of the BELLE flavor tagging group for their generous cooperation. I am specially grateful to Prof. Y. Sakai, Dr. H. Hamasaki, Dr. J. Suzuki and Mr. T. Okabe.

I also owe a lot to the members of the Nagashima Group at Osaka University for the good companionship and encouragement. Dr. T. Kawasaki, Dr. K. Senyo, Mr. K. Sumisawa, Mr. S. Hidaka, Mr. M. Yoshida, Mr. J. Ryuko and Mr. T. Houjo have given me a great deal of help to proceed in my research. I am very much thankful to my colleagues Mr. K. Nitta, Mr. K. Manabe and Mr. H. Miyake for their kindness and friendship. I also thank to my colleagues Ms. Y. Kajiyama, Mr. M. Matumoto, Mr. H. Tagomori, Ms. Y. Ikemoto, Mr. T. Ishikawa, Mr. K. Kurahata and Mr. M. Tuchihashi. I enjoyed the life at the university with them. I am very indebted to Ms. S. Tsuzuki for her encouragement and help. I also would like to thank all the members of the BELLE collaboration and the KEKB accelerator group for keeping the experiment stable and providing excellent data.

Abstract

We studied flavor tagging of neutral B meson at the KEK B-factory. Flavor tagging is an essential technique needed to measure the CP violation in the B meson system. There are two requirements for flavor tagging. One is to maximize the effective efficiency, and the other is to estimate the wrong tagging fraction precisely.

To maximize the effective efficiency, we performed Monte Carlo simulation and obtained an effective efficiency of $25.05 \pm 0.07\%$ with leptons and charged kaons.

To estimate the wrong tagging fraction, we established a method using $B^0(\overline{B^0}) \to D^{*\mp} l^{\pm} \nu$ decays in place of the CP decay and confirmed that using this method we can estimate the wrong tagging fraction with enough accuracy for CP violation measurement.

Contents

Chapter 1

Introduction

The KEK B-factory is an experiment which started taking data in 1999 and is now in operation at the High Energy Accelerator Research Organization (KEK) in Tsukuba, Japan. The primary goal of the KEK B-factory experiment is to observe CP violation in B meson decays in e^+e^- collisions at the energy of the $\Upsilon(4S)$ resonance and to perform a test of the Standard Model. In this chapter, we describe the role of flavor tagging in the CP violation measurement and set the goal of this thesis.

1.1 CP violation

In 1964, CP violation was discovered by Christenson, Cronin, Fitch and Turlay[1] in neutral K decays. Before the discovery, while C and P were already known to be broken, it was believed that CP, which is a combination of them, was still invariant. They found long-lived neutral K mesons, which were supposed to have $CP = -1$, decayed to $\pi^+\pi^-$, which has $CP = +1$. After that CP violation in K mesons has been confirmed by other experiments through other decay modes. However no one has observed CP violation in other systems. The physics of B decays is expected to be another field of CP violation study.

One of the most notable theories to explain the origin of CP violation is the theory of Kobayashi and Maskawa published in 1973[2]. They claimed that if there were at least six quark flavors, CP violation could be introduced to the Standard Model without any modification. They pointed out that the mixing matrix among more than or equal to six quark flavors must have a complex term which was necessary to cause CP violation.

We can represent the Kobayashi-Maskawa matrix by

$$\begin{pmatrix} d' \\ s' \\ b' \end{pmatrix} = \begin{pmatrix} V_{ud} & V_{us} & V_{ub} \\ V_{cd} & V_{cs} & V_{cb} \\ V_{td} & V_{ts} & V_{tb} \end{pmatrix} \begin{pmatrix} d \\ s \\ b \end{pmatrix}. \tag{1.1}$$

A requirement that this matrix must be unitary leads to the equation

$$V_{ud}V_{ub}^* + V_{cd}V_{cb}^* + V_{td}V_{tb}^* = 0. \tag{1.2}$$

This relation can be expressed as a triangle called the unitarity triangle, on the complex plane shown in figure 1.1. Three angles are defined as

$$\phi_1 = \pi - \arg\left(\frac{-V_{td}V_{tb}^*}{-V_{cb}^*V_{cd}}\right), \phi_2 = \arg\left(\frac{V_{tb}^*V_{td}}{-V_{ub}^*V_{ud}}\right), \phi_3 = \arg\left(\frac{V_{ub}^*V_{ud}}{-V_{cb}^*V_{cd}}\right). \tag{1.3}$$

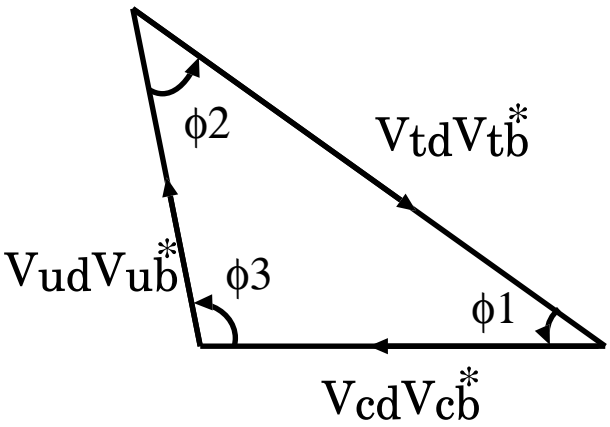

Figure 1.1: The unitarity triangle of the KM matrix.

To test the Kobayashi-Maskawa theory, it is necessary to measure the lengths of 3 sides and the magnitudes of 3 angles precisely. In the case of the K meson system, terms which include b and t quarks are difficult to measure, because it includes them as higher order terms. For the B meson system, since it includes the b quark, the terms can be measured more explicitly.

Therefore experiments on the B meson system are essential to establish not only the Kobayashi-Maskawa theory but also the Standard Model.

1.2 CP violation in B decays

In B decays, one of the methods to detect CP violation is to measure the difference of a time dependent decay rate between B^0 and $\overline{B^0}$ decaying to a certain CP eigenstate common to B^0 and $\overline{B}^0$. This asymmetry is directly related to an angle in the unitarity triangle. This CP violation is caused by the interference of mixing and decay. In this section, we briefly explain the mechanism.

1.2.1 $B^0\overline{B}^0$ mixing

B^0 and $\overline{B}^0$ can mix through second order weak interactions known as the "Box Diagrams" (figure 1.2). Therefore an arbitrary neutral meson state is written as the admixture, $a|B^0\rangle + b|\overline{B}^0\rangle$, which is governed by the time-dependent Schrödinger equation

$$i\frac{d}{dt}\begin{pmatrix} a \\ b \end{pmatrix} = \left(M - \frac{i}{2}\Gamma\right)\begin{pmatrix} a \\ b \end{pmatrix}. \tag{1.4}$$

Here M and Γ are Hermitian 2×2 matrices, which are called the mass and decay matrices, respectively. The two mass eigenstates B_H and B_L (H means heavy mass and L means light mass) are given by

$$\begin{aligned} B_L &= p|B^0\rangle + q|\overline{B}^0\rangle, \\ B_H &= p|B^0\rangle - q|\overline{B}^0\rangle, \end{aligned} \tag{1.5}$$

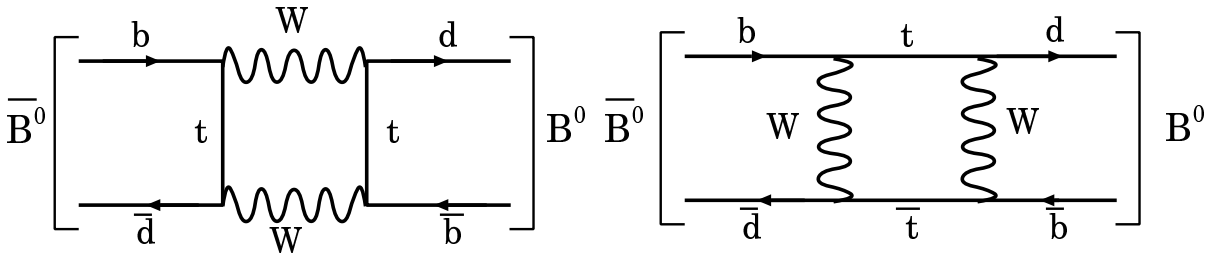

Figure 1.2: Box diagrams for $B^0 - \overline{B}^0$ mixing in the Standard Model

where

$$\frac{q}{p} = \sqrt{\frac{M_{12}^* - \frac{i}{2}\Gamma_{12}^*}{M_{12} - \frac{i}{2}\Gamma_{12}}}. \tag{1.6}$$

The time evolution of these states is given by

$$\begin{aligned} |B_L(t)\rangle &= e^{-iM_L t} e^{-\frac{\Gamma_L t}{2}} |B_L(0)\rangle, \\ |B_H(t)\rangle &= e^{-iM_H t} e^{-\frac{\Gamma_H t}{2}} |B_H(0)\rangle. \end{aligned} \tag{1.7}$$

In the B meson system, we can neglect the difference of the width between B_L and B_H, $\Gamma_L = \Gamma_H = \Gamma$, because the difference is produced by common decay channels to B^0 and $\overline{B}^0$ with branching ratios of order 10^{-3} or less. On the other hand the mass difference, $\Delta M = M_H - M_L$, is measured to be $\Delta M/\Gamma \sim 0.7$. From these facts it follows that $\Gamma_{12}/M_{12} \ll 1$ and ratio of q to p becomes

$$\left|\frac{q}{p}\right| \simeq \left|\frac{M_{12}^*}{M_{12}}\right| \sim 1. \tag{1.8}$$

Pure B^0 and $\overline{B}^0$ states are

$$\begin{aligned} |B^0\rangle &= \tfrac{1}{2p}(|B_H\rangle + |B_L\rangle), \\ |\overline{B}^0\rangle &= \tfrac{1}{2q}(|B_H\rangle - |B_L\rangle). \end{aligned} \tag{1.9}$$

With definitions that $M \equiv (M_L + M_H)/2$ and $\Delta M \equiv M_H - M_L$, the time evolution of an initially pure B^0 or $\overline{B}^0$ state is given by

$$\begin{aligned} |B^0(t)\rangle &= e^{-iMt} e^{-\frac{1}{2}\Gamma t} \left\{ \cos\left(\tfrac{1}{2}\Delta M t\right) |B^0\rangle \ + \tfrac{iq}{p} \sin\left(\tfrac{1}{2}\Delta M t\right) |\overline{B}^0\rangle \right\}, \\ |\overline{B}^0(t)\rangle &= e^{-iMt} e^{-\frac{1}{2}\Gamma t} \left\{ \tfrac{ip}{q} \sin\left(\tfrac{1}{2}\Delta M t\right) |B^0\rangle + \cos\left(\tfrac{1}{2}\Delta M t\right) |\overline{B}^0\rangle \ \right\}. \end{aligned} \tag{1.10}$$

1.2.2 CP violation in the interference of mixing and decay

Consider decays of neutral B mesons to a CP eigenstate, f_{cp}. The amplitudes for these processes are defined as

$$\begin{aligned} A &\equiv \langle f_{CP}|\mathcal{H}|B^0\rangle, \\ \overline{A} &\equiv \langle f_{CP}|\mathcal{H}|\overline{B}^0\rangle. \end{aligned} \tag{1.11}$$

We define another quantity for convenience

$$\lambda \equiv \frac{q}{p}\frac{\overline{A}}{A}. \tag{1.12}$$

If there is no direct CP violation, $|\lambda|$ is 1.

Using equation (1.10), the time-dependent decay rates of initially pure B^0 or $\overline{B}^0$ states become

$$\begin{aligned}\Gamma(B^0(t) \to f_{CP}) &= |A^2|e^{-\Gamma t}\left\{\tfrac{1+|\lambda|^2}{2} + \tfrac{1-|\lambda|^2}{2}\cos\Delta Mt - \mathrm{Im}\lambda \sin\Delta Mt\right\}, \\ \Gamma(\overline{B}^0(t) \to f_{CP}) &= |A^2|e^{-\Gamma t}\left\{\tfrac{1+|\lambda|^2}{2} - \tfrac{1-|\lambda|^2}{2}\cos\Delta Mt + \mathrm{Im}\lambda \sin\Delta Mt\right\}.\end{aligned} \tag{1.13}$$

If we define the CP asymmetry as

$$a_{f_{CP}} \equiv \frac{\Gamma(\overline{B}^0(t) \to f_{CP}) - \Gamma(B^0(t) \to f_{CP})}{\Gamma(\overline{B}^0(t) \to f_{CP}) + \Gamma(B^0(t) \to f_{CP})}, \tag{1.14}$$

and if $|\overline{A}/A| = 1$ and $|\lambda| = 1$ are satisfied, we obtain

$$a_{f_{CP}} = \mathrm{Im}\lambda \times \sin\Delta Mt. \tag{1.15}$$

The quantity $\mathrm{Im}\lambda$ which can be extracted from $a_{f_{CP}}$ is theoretically very interesting since it can be directly related to Kobayashi-Maskawa matrix elements in the Standard Model.

1.2.3 $B^0(\overline{B}^0) \to J/\psi K_s$ mode

One of the CP eigenstates which B mesons decay to is $J/\psi K_s$ ($CP = -1$).

In equation (1.8), M_{12} represents an amplitude of transition of $\overline{B}^0 \to B^0$ and $B^0 \to \overline{B}^0$ via top quarks as in Fig. 1.2. Therefore q/p is given by

$$\frac{q}{p} \simeq \frac{M_{12}^*}{M_{12}} = \frac{V_{td}V_{tb}^*}{V_{tb}V_{td}^*}. \tag{1.16}$$

The decay $B^0(\overline{B}^0) \to J/\psi K_s$ is expressed by the diagram shown in figure 1.3, and $\overline{A}/A$ is

$$\frac{\overline{A}}{A} = \frac{V_{cb}V_{cs}^*}{V_{cb}^*V_{cs}}. \tag{1.17}$$

In addition, considering mixing of the neutral K meson, λ becomes

$$\lambda = -\frac{V_{tb}^*V_{td}}{V_{tb}V_{td}^*}\frac{V_{cs}^*V_{cb}}{V_{cs}V_{cb}^*}\frac{V_{cd}^*V_{cs}}{V_{cd}V_{cs}^*}. \tag{1.18}$$

As λ is related to the angle ϕ_1 in figure 1.1,

$$\mathrm{Im}\lambda = \sin 2\phi_1, \tag{1.19}$$

the asymmetry (1.15) becomes

$$a_{f_{CP}} = \sin 2\phi_1 \times \sin\Delta Mt. \tag{1.20}$$

Therefore we can determine the angle ϕ_1 directly by measuring the asymmetry. Because $B^0(\overline{B}^0) \to J/\psi K_s$ is expected to be almost free from backgrounds and to have negligible theoretical uncertainty, this decay is the most promising process to observe CP violation in B decays and is called the "Gold-Plated Mode".

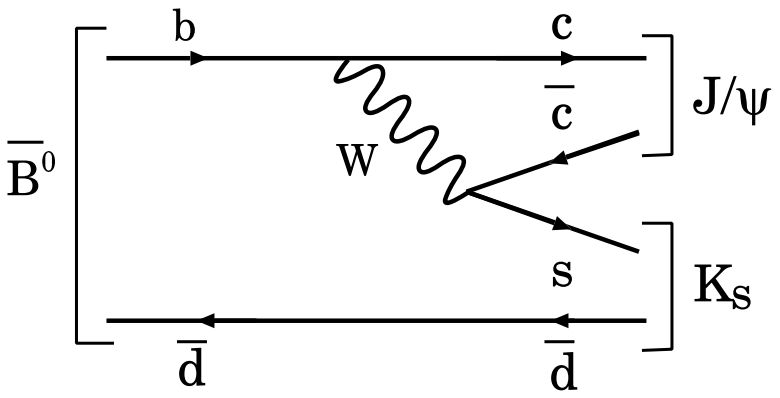

Figure 1.3: Diagram for the decay $\overline{B}^0 \to J/\Psi K_s$

1.3 Flavor tagging

To observe the CP violation mentioned in the previous section, we need to know the initial state of the B meson. Since it is impossible to distinguish B^0 from $\overline{B}^0$ with the flavor non-specific final state, it is essential to use other information. In experiments using B mesons, this determination is usually called "flavor tagging".

Flavor tagging technique is generally divided into two categories:

- One is the same-side tagging. This technique is used in experiments which have much higher energy than the production threshold of a $B\overline{B}$ meson pair. In such experiments, a $b\overline{b}$ quark pair makes two (or more) jets and a $B(\overline{B})$ meson is generated in the $\overline{b}(b)$ quark jets. This technique uses the correlation between the flavor of a B meson and the charge of a nearby particle in the jet which the B meson belongs to. This correlation arises from the fragmentation processes which form a B meson from a b quark, as well as pions from an excited state of a B meson. At the KEK B-factory, the center of mass energy is $10.58 GeV/c^2$, corresponding to the mass of the $\Upsilon(4S)$, which is only 20 MeV/c^2 above the production threshold of a $B\overline{B}$ meson pair. Therefore this technique is not available at the KEK B-factory and another method is used.

- Another one is the opposite-side tagging. This method employs the fact that b and $\overline{b}$ quarks are produced as a pair and tags the flavor of the opposite-side B meson. In this thesis, we call this opposite side the tagging-side and the tagging-side B meson is denoted by B_{tag}. The other side decaying into a CP eigenstate is called CP side and denoted by B_{cp}.

At the KEK B-factory, B mesons are generated as a pair of B^0 and $\overline{B}^0$ from $\Upsilon(4S)$ resonance. This B meson pair is produced in a coherent $B^0\overline{B}^0$ state and remains in this state until one of them decays. Thanks to this coherent time evolution, if B_{tag} decays first and if we can tag the flavor of B_{tag}, the initial flavor of B_{cp} is fixed to the opposite flavor of B_{tag} (figure 1.4).

If B_{cp} decays first, the situation is different. However, we can treat both cases with an

asymmetry redefined as[3],

$$
\begin{aligned}
a_{f_{CP}} &\equiv \frac{\Gamma(B_{tag} \to B^0(t'), B_{cp} \to f_{CP}(t)) - \Gamma(B_{tag} \to \overline{B}^0(t'), B_{cp} \to f_{CP}(t))}{\Gamma(B_{tag} \to B^0(t'), B_{cp} \to f_{CP}(t)) + \Gamma(B_{tag} \to \overline{B}^0(t'), B_{cp} \to f_{CP}(t))}, \\
&= \mathrm{Im}\lambda \sin(\Delta M \Delta t),
\end{aligned}
\tag{1.21}
$$

where $\Delta t \equiv t - t'$ and $\Gamma(B_{tag} \to B^0(\overline{B}^0)(t'), B_{cp} \to f_{CP}(t))$ is the decay rate of B_{tag} into $B^0(\overline{B}^0)$ at t' and of B_{cp} into f_{CP} at t, respectively. The case that B_{tag} decays first corresponds to positive Δt and negative Δt corresponds to the case when B_{tag} decays after the decay of B_{cp}. Figure 1.5 shows the proper time distribution for $f_{CP} = J/\psi Ks$ with $\sin 2\phi_1 = 0.6$.

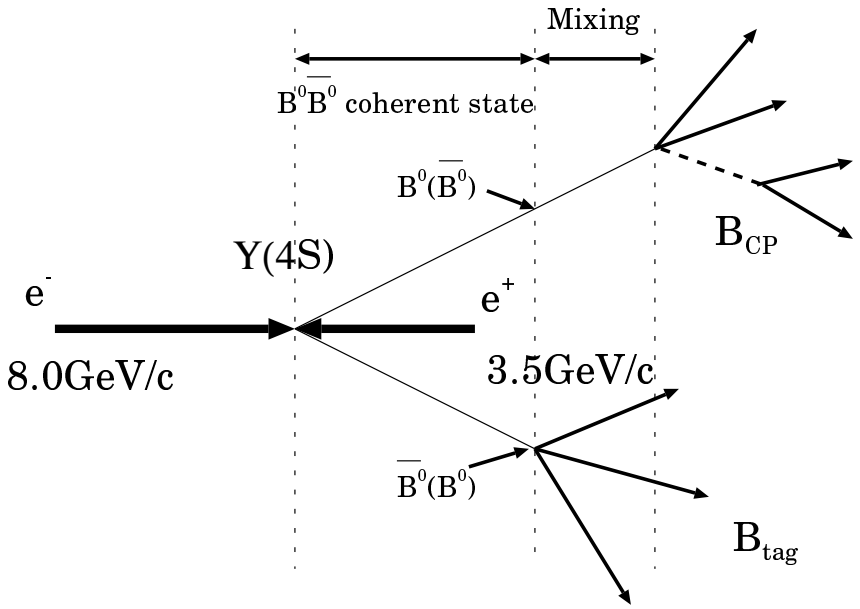

Figure 1.4: Example of $B^0\overline{B}^0$ decay. If B_{tag} is $B^0(\overline{B}^0)$, B_{cp} is $\overline{B^0}(B^0)$ at the time when B_{tag} decays.

Therefore at the KEK B-factory experiment, flavor tagging is regarded as the determination of the flavor of B_{tag}. After full reconstruction of B_{cp} and the removal of the decay products of B_{cp}, since the rest of the event consists only of the decay products of B_{tag}, flavor tagging can also be defined as a technique to tag the flavor of a single neutral B meson decaying generically.

1.4 Flavor tagging with leptons and charged K mesons

To tag the flavor of B_{tag}, leptons and charged K mesons are good tools. Leptons and charged kaons mainly come from decays of b-quarks through the diagrams shown in figure 1.6. The charge of particles is related to the flavor of B_{tag}, i.e. if the charge is $+1(-1)$, the flavor of B_{tag} is $B^0(\overline{B}^0)$.

There are other sources of leptons and charged K mesons as shown in figure 1.7. These particles as well as particles misidentified as leptons or charged K mesons cause wrong tagging and affect CP violation measurement.

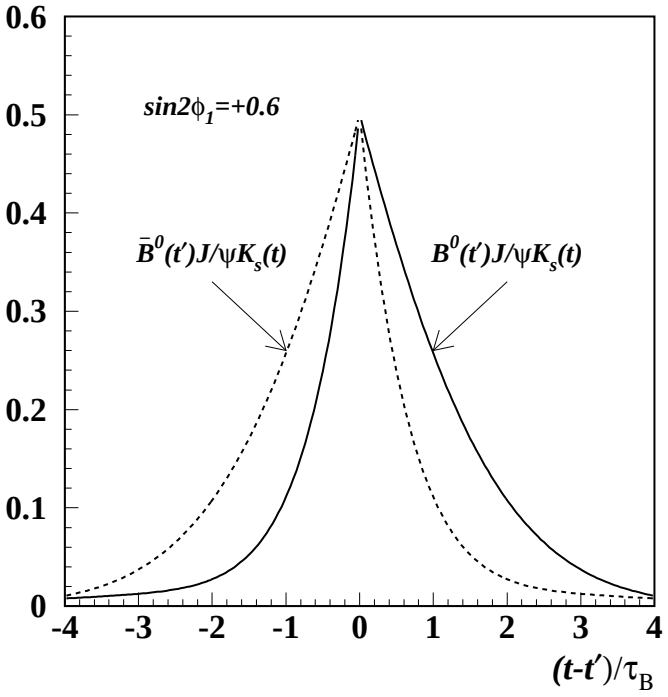

Figure 1.5: Proper time distribution for $B^0\overline{B}^0 \to J/\psi Ks$.

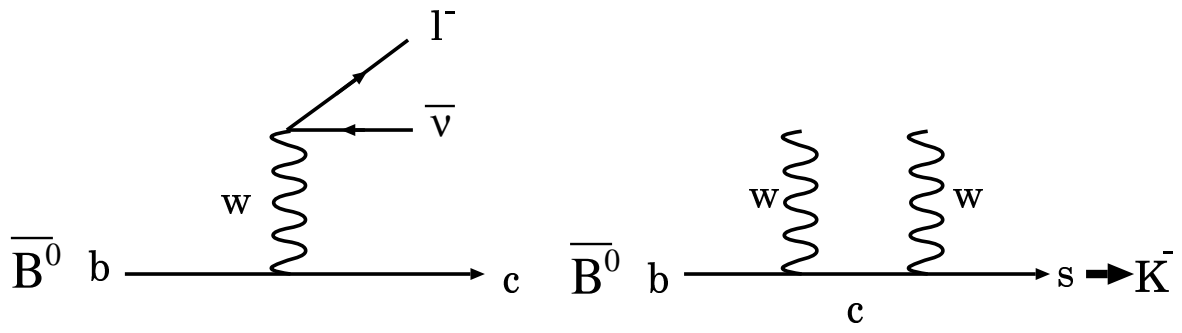

Figure 1.6: Flavor specific decay of $\overline{B}^0$. Semileptonic decay of a b-quark (left). A kaon originating from cascade decay of a b-quark to a s-quark (right).

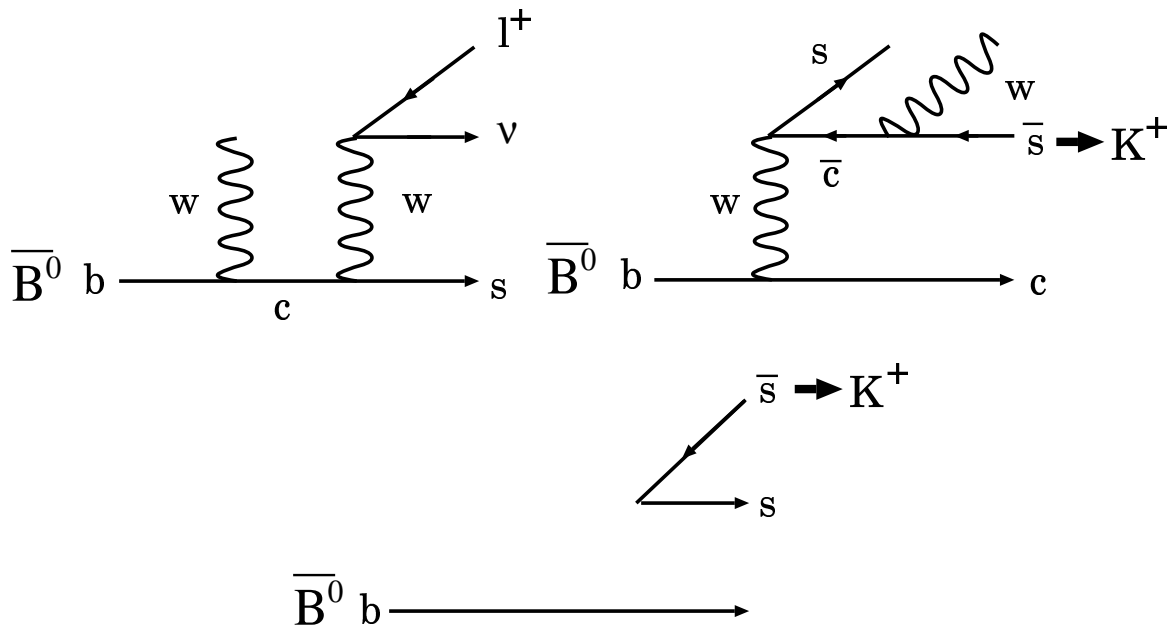

Figure 1.7: Main sources of wrong tagging. A lepton from the cascade decay of c-quark (left). A kaon originating from $W \to \overline{c}s$ transition (right). A kaon from $s\overline{s}$ popping in the hadronization phase (lower).

We define the efficiency of flavor tagging (ϵ) as

$$\epsilon = \frac{\text{Number of flavor-tagged events}}{\text{Number of events}}. \tag{1.22}$$

This is the probability that the flavor of B_{tag} is determined. This includes wrongly-tagged events. We express the fraction of wrongly-tagged events (ω) as

$$\text{wrong tagging fraction } \omega = \frac{\text{Number of wrongly-tagged events}}{\text{Number of flavor-tagged events}}. \tag{1.23}$$

1.5 Requirement for flavor tagging

As described in the previous section, there exists a wrong tagging fraction ω in flavor tagging which dilutes the measured asymmetry ($A_{measured}$);

$$A_{measured} = (1 - 2\omega) \times a_{f_{CP}}. \tag{1.24}$$

Considering this dilution, the statistical significance of the asymmetry is given by

$$\text{significance} = \frac{A_{measured}}{\delta A_{measured}} \propto \sqrt{\epsilon(1-2\omega)^2 \times N_{cp}}, \tag{1.25}$$

where N_{cp} is the number of reconstructed B_{cp} events. Since $\epsilon(1-2\omega)^2$ effectively works as the efficiency for flavor tagging in the statistical significance of the measured asymmetry, we define this quantity as the effective efficiency,

$$\epsilon_{eff} \equiv \epsilon(1-2\omega)^2. \tag{1.26}$$

These equations lead to two requirements for flavor tagging:

- maximize ϵ_{eff}

  We must optimize the method of flavor tagging to maximize ϵ_{eff}.

- estimate ω precisely

  Due to dilution, the uncertainty of ω gives a systematic error to the CP asymmetry as follows:

  $$\delta a_{f_{CP}} = a_{f_{CP}} \times \frac{\delta(1-2\omega)}{(1-2w)}. \tag{1.27}$$

  Therefore it is very important to estimate ω precisely.

1.6 Goal of this study

Flavor tagging is an essential technique to measure CP violation in B decays. To satisfy the requirements we mentioned in the previous section, we set the goal of our study as follows:

- Perform Monte Carlo simulation study to estimate how much ϵ_{eff} we can achieve with kaons and leptons.

- Establish a method to estimate ω and apply it to real data collected at KEK B-factory.

The outline of this thesis is as follows: In chapter 2, we give an overview of the experimental apparatus at the KEK B-factory. In chapter 3, we describe a Monte Carlo simulation study of flavor tagging. In chapter 4, the estimation of ω with Monte Carlo and real data is explained. Finally, the conclusion is given in chapter 5.

Chapter 2

KEK B-factory

In this chapter, we describe the experimental apparatus at the KEK B-factory, the KEKB accelerator and the BELLE detector.

2.1 KEKB accelerator

KEKB [4] is an electron-positron collider. The energy of electrons and positrons are $8GeV$ and $3.5GeV$, respectively. The center-of-mass energy is $10.58GeV$, which corresponds to the $\Upsilon(4S)$ resonance. Asymmetric energy is chosen to boost the B mesons to ease the measurement of their decay length. The design luminosity is $10^{34}cm^{-2}s^{-1}$ in order to produce 10^8 $\Upsilon(4S)$ a year.

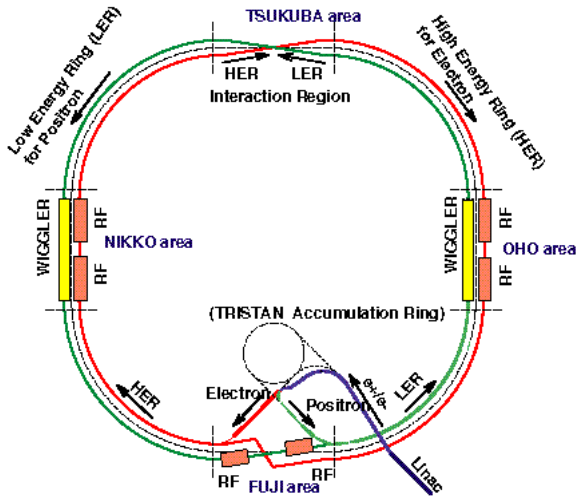

Figure 2.1: Configuration of the KEKB accelerator system.

Figure 2.1 illustrates the configuration of the two rings of KEKB. The electron ring is called the HER (High Energy Ring) and the positron ring is called the LER (Low Energy Ring). These rings are built side by side in the existing TRISTAN tunnel, which has a circumference of about $3km$. KEKB has only one interaction point in the Tsukuba experimental hall, where the electron and positron beams collide at a finite angle of $\pm 11mrad$. The BELLE detector is installed at

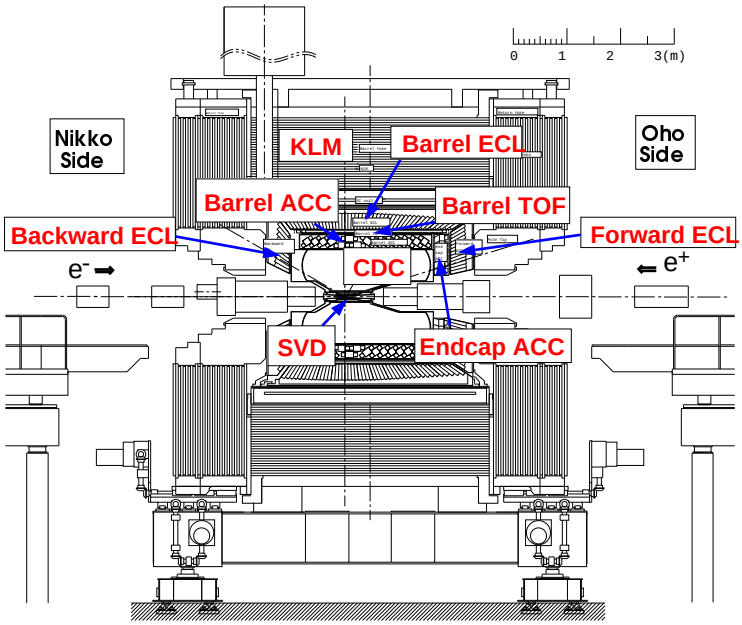

Figure 2.2: BELLE detector

this interaction region. To achieve the design luminosity, 5000 bunches are injected into each ring. The main parameters of KEKB are summarized in table 2.1.

2.2 BELLE detector

The configuration of the BELLE detector [5] is shown in figure 2.2.

The asymmetric design of the detector reflects the asymmetry of the beam energy. The detector has a larger acceptance in the direction of the electrons, which is defined as "the forward region", than in the direction of the positrons, which is defined as "the backward region". The definition of the regions and the axis of the coordinates are shown in figure 2.3. The BELLE detector consists of six detectors and a solenoid magnet. The detectors are, in order from the inside, the silicon vertex detector (SVD) for B meson vertexing, the central drift chamber (CDC) for tracking and dE/dx measurement, the aerogel Čherenkov counter (ACC), the time of flight counter (TOF) and the electromagnetic calorimeter (ECL),for particle identification, the super conducting solenoid for momentum measurement and the K_L meson and muon counter (KLM). The expected performance of each detector is summarized in table 2.2. A brief description of the detector components follows.

2.2.1 SVD

The SVD has three cylindrical layers each consisting of units of the Double-Sided Silicon Detectors (DSSD's). Each DSSD has size of $57.5mm \times 33.5mm$ and a thickness of $300\mu m$. One side of the DSSD has 1280 $42\mu m$-spaced n^+-strips oriented perpendicular to the beam direction to measure the z coordinate. The n^+-strips are interleaved by p^+ implants. Each pair of n^+-strips is connected to a single readout channel. The other side of the DSSD has 1281 $25\mu m$-spaced

Ring		LER	HER	
Energy	E	3.5	8.0	GeV
Circumference	C	3016.26		m
Luminosity	$\mathcal{L}$	1×10^{34}		$\mathrm{cm}^{-2}\mathrm{s}^{-1}$
Crossing angle	θ_x	± 11		mrad
Tune shifts	ξ_x/ξ_y	0.039/0.052		
Beta function at CP	β_x^*/β_y^*	0.33/0.01		m
Beam current	I	2.6	1.1	A
Natural bunch length	σ_z	0.4		cm
Energy spread	σ_ε	7.1×10^{-4}	6.7×10^{-4}	
Bunch spacing	s_b	0.59		m
Particle/bunch	N	3.3×10^{10}	1.4×10^{10}	
Emittance	$\varepsilon_x/\varepsilon_y$	$1.8 \times 10^{-8}/3.6 \times 10^{-10}$		m
Synchrotron tune	ν_s	$0.01 \sim 0.02$		
Betatron tune	ν_x/ν_y	45.52/45.08	47.52/43.08	
Momentum compaction factor	α_p	$1 \times 10^{-4} \sim 2 \times 10^{-4}$		
Energy loss/turn	U_o	0.81†/1.5‡	3.5	MeV
RF voltage	V_c	$5 \sim 10$	$10 \sim 20$	MV
RF frequency	f_{RF}	508.887		MHz
Harmonic number	h	5120		
Longitudinal damping time	τ_ε	43†/23‡	23	ms
Total beam power	P_b	2.7†/4.5‡	4.0	MW
Radiation power	P_{SR}	2.1†/4.0‡	3.8	MW
HOM power	P_{HOM}	0.57	0.15	MW
Bending radius	ρ	16.3	104.5	m
Length of bending magnet	ℓ_B	0.915	5.86	m

†: without wigglers, ‡: with wigglers

Table 2.1: Main parameters of KEKB.

Detector	Type	Configuration	Readout	Performance
Beam pipe	Beryllium double-wall	Cylindrical, r=2.3 cm 0.5mm Be/2mm He /0.5mm Be		Helium gas cooled
SVD	Double Sided Si Strip	300 μm-thick, 3 layers r = 3.0 - 5.8 cm Length = 22 - 34 cm	81.9 K	$\sigma_{\Delta z} \sim 105$ μm
CDC	Small Cell Drift Chamber	Anode: 52 layers Cathode: 3 layers r = 8.5 - 90 cm -77$\leq z \leq$ 160 cm	A: 8.4 K C: 1.5 K	$\sigma_{r\phi} = 130$ μm $\sigma_z = 200 \sim 1,400\mu$m σ_{p_t}/p_t =0.3%$\sqrt{p_t^2+1}$ $\sigma_{dE/dx} = 6\%$
ACC	n : 1.01 $\sim$ 1.03 Silica Aerogel	$\sim$12x12x12 cm^3 blocks 960 barrel / 228 endcap FM-PMT readout	1,788	$\mu_{eff} \geq 6$ K/π 1.2<p<3.5GeV/c
TOF	Scintillator	128 ϕ segmentation r = 120 cm, 3 m-long	128$\times$2	σ_t = 100 ps K/π up to 1.2GeV/c
ECL	CsI	Towered structure $\sim$ 5.5x5.5x30 cm^3 crystals Barrel: r = 125 - 162 cm Endcap: z = -102 and +196 cm	6,624 1,152(f) 960(b)	σ_E/E= 0.67%/$\sqrt{E}\oplus$1.8% σ_{pos}=0.5 cm/$\sqrt{E}$ E in GeV
MAGNET	super conducting	inn.rad. = 170 cm		B = 1.5 T
KLM	Resistive Plate c.	14layers (5cm Fe+4cm gap) two RPCs in each gap θ and ϕ strips	θ:16 K ϕ:16 K	$\Delta\phi$=$\Delta\theta$=30mr for K_L σ_t=1ns 1% hadron fakes

Table 2.2: Performance parameters of the BELLE detector.

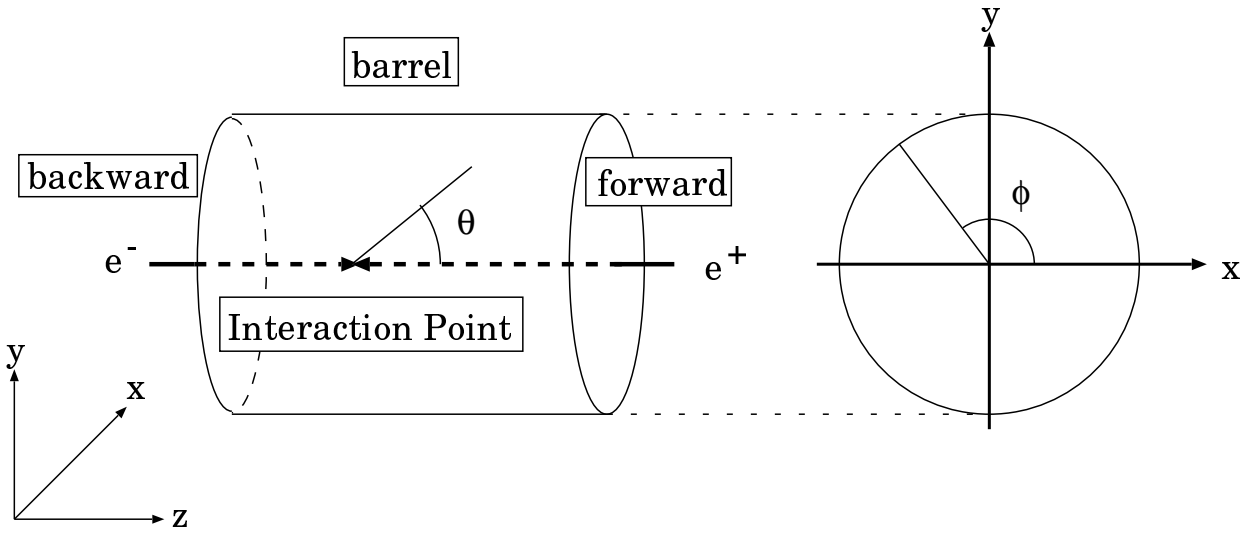

Figure 2.3: Definition of the axis of the coordinates.

longitudinal p^+-strips which provide the ϕ coordinate measurement. Every second p^+-strip is connected to a single readout channel. The position of each layer is at $3.0cm$, $4.55cm$ and $6.05cm$ in the radial direction. The three layers have 8, 10 and 14 sensor ladders in ϕ, respectively. The sensor ladders have 2, 3 and 4 DSSD's to cover the acceptance of 21 to 140 degree in polar angle in layer 1, 2 and 3, respectively. The SVD has 102 DSSD's in total with a total of 81,920 readout channels.

2.2.2 CDC

The CDC is a cylindrical drift chamber with small square cells. It consists of 3 parts, Cathode, Inner and Main part. The chamber has an acceptance of 17 to 150 degrees in polar angle. The longest wires are $2400mm$ long. The outer radius is $88cm$ and the inner radius of the main part is $28cm$ from the beam line. The inner part covers the radial region from $28cm$ to $9cm$. The inner radius of the CDC extend down to $8.3cm$ from the beam line, without any walls, to include the cathode part. For readout, the chamber has 50 cylindrical layers organized in 11 super-layers, including 6 axial layers and 5 stereo layers. Each stereo super-layer has 4 layers of sense wires. In total 8,400 readout channels are used for sense wires and 24,944 wires are used for field wires. Each sense wire is $30\mu m$ in diameter and is made of tungsten plated with gold. Field wires with a diameter of $126\mu m$ are made of aluminum.

2.2.3 ACC

The ACC is a threshold Čherenkov counter system. Each aerogel counter module consists of a silica aerogel radiator module and fine-mesh photomultiplier tubes to detect Čherenkov radiation. The ACC consists of a barrel part and a forward endcap part. The barrel part of the ACC has 960 aerogel counters; 16-fold segmentation in z and 60-fold segmentation in ϕ. Five different indices of refraction, $n = 1.01$, 1.013, 1.015, 1.020 and 1.028, are used depending on θ.

Each barrel counter is viewed by one or two fine-mesh photo-multipliers (FM-PMT). The endcap part of the ACC has 228 counters in total with $n = 1.03$ and is structured in five concentric rings with 36-, 38, 48-, 48-, and 60-fold segmentation from inside to outside. Each endcap counter is viewed by one FM-PMT through an air light guide. The number of readout channels is 1,560 in the barrel and 228 in the endcap.

2.2.4 TOF and trigger

One layer of $5mm$-thick Trigger Scintillation Counter (TSC) and two layers of $4cm$-thick Time of Flight counters (TOF) separated by a $2cm$ gap are located at $r = 120cm$. The TOF is segmented into 128 ϕ sectors and read out by one FM-PMT at each end. The TSC's have 64-fold segmentation and are read out from the backward end only by a single FM-PMT. The number of readout channels is 256 for the TOF and 64 for the TSC.

2.2.5 ECL

The ECL consists of arrays of $\mathrm{CsI}(\mathrm{T}l)$ crystals with silicon photodiode readout installed inside the coil of the solenoid magnet. All $\mathrm{CsI}(\mathrm{T}l)$ crystals are $30cm$ (16.1 radiation lengths) long, and are assembled into a tower structure pointing towards the interaction point. The barrel part of the ECL has 46-fold segmentation in θ and 144-fold segmentation in ϕ. The forward (backward) endcap part of the ECL has 13-(10-) fold segmentation in θ and the ϕ segmentation varies from 48 to 144 (64 to 144). The barrel part has 6,624 crystals and the forward (backward) endcap part has 1,152(960) crystals. Each crystal is read out by two $10mm \times 20mm$ photo-diodes. The total number of readout channel is 17,472. The inner radius of the barrel part is $125cm$. The forward (backward) endcap part starts at $z = +196cm(-102cm)$.

2.2.6 Solenoid magnet

The solenoidal magnet provides an axial magnetic field of about 1.5 Tesla over the tracking volume of BELLE. The coil consists of a single layer of an aluminum-stabilized superconductor coil, a niobium-titanium-copper alloy embedded in a high purity aluminum stabilizer. Indirect cooling is provided by liquid helium circulating through a single tube welded on the outersurface of the support structure.

2.2.7 KLM

The KLM detector consists of a barrel part and two endcap parts. The KLM consists of a sandwich of fourteen $4.7cm$-thick iron absorber plates and fourteen RPC (Resistive Plate Counter) superlayers. The barrel part of the KLM has one additional RPC superlayer inside the innermost iron plate. The iron also serves as the flux return for the magnetic field provided by the solenoid. Each RPC superlayer consists of two RPCs and provides two dimensional information. The RPC is a kind of a planar spark chamber which detects the avalanche induced by an incident charged particle. The RPC is made of $2mm$ thick glass electrodes. Signals are read out by $\sim 5cm$-wide cathode strips in both θ and ϕ. The number of readout channels is 21,856 in the barrel and 16,128 in the endcap.

Chapter 3

Monte Carlo Simulation

In this chapter we presents a Monte Carlo simulation study of flavor tagging. In section 3.1, we briefly outline the simulation. In section 3.2, the simplest method with high momentum leptons and kaons is studied. In the rest of the sections, we focus on getting higher effective efficiency with flavor tagging for leptons. In section 3.3, we utilize the missing momentum and the lepton momentum simultaneously. In section 3.4, we investigate the feasibility of utilizing low momentum leptons. Last of all, the overall effective efficiency is estimated in 3.5.

3.1 Outline

We generate 10^6 $B^0\overline{B}^0$ events with the event generator QQ [6] which has been developed by the CLEO group and designed to simulate e^+e^- collisions at the energy of the $\Upsilon(4S)$. As mentioned in section 1.3, flavor tagging at the KEK B-factory is equivalent to tagging the flavor of a single B meson decaying generically. Therefore in this study we mask out one of the B mesons and let the other B meson decay generically[1] .

The generated particles are put into the detector simulator based on GEANT[7], which was followed by the BELLE event reconstruction program[2] .

Then we applied flavor tagging and compared the results with the true flavor in the generator to estimate ϵ, ω, ϵ_{eff}.

3.2 Flavor tagging with high momentum lepton and kaons

As described in section 1.4, the flavor of B_{tag} can be tagged with either leptons from the semileptonic B decay or kaons in the cascade decay.

Leptons from semileptonic B decay have higher momentum in the $\Upsilon(4S)$ center of mass system (p_l^*) than other leptons. Figure 3.1 shows the distribution of p_l^* at the level of the event generator. There is a clear difference between leptons from B semileptonic decay and other leptons. For kaons, the charge sum of kaons (denoted by $\sum Q_K$) has a strong correlation with the flavor of their parent B meson. Figure 3.2 shows the distribution of $\sum Q_K$ for neutral B decays at the level of the event generator.

We apply the following criteria:

[1] One B was forced to decay into $\nu\overline{\nu}$ in order to mask it out.

[2] We use the library of September, 1999 version.

p_l^* cut	total ϵ_{eff} with leptons and kaons
1.4 GeV/c	23.12 ± 0.07 %
1.3 GeV/c	23.73 ± 0.07 %
1.2 GeV/c	24.08 ± 0.07 %
1.1 GeV/c	24.14 ± 0.07 %
1.0 GeV/c	23.84 ± 0.07 %
0.9 GeV/c	23.13 ± 0.07 %

Table 3.1: The p_l^* cut dependence of total ϵ_{eff} with leptons and kaons

1. Find a high momentum lepton. Then the relations $B_{tag} = B^0$ for l^+ and $B_{tag} = \overline{B}^0$ for l^- are used.

2. If no high momentum lepton is found or there are more than one high momentum leptons, we examine the charge sum of the kaons. Then we determine the flavor of B_{tag} by using the relations $B_{tag} = B^0$ for $\sum Q_K > 0$ and $B_{tag} = \overline{B}^0$ for $\sum Q_K < 0$.

Since flavor tagging with a high momentum lepton is expected to have smaller ω than that with kaons, we choose this order.

We identify muons with the KLM and electrons with the combined information from CDC,ACC,TOF and ECL. We tag kaons by using combined information from CDC,ACC and TOF. The distribution of reconstructed the p_l^* is shown in figure3.3. We choose leptons with $p_l^* > 1.1 GeV/c$ to select primary leptons to obtain the best effective efficiency (table 3.1). The charge sum of kaons is shown in figure 3.4. The results are summarized in table 3.2. The difference between B^0 and $\overline{B}^0$ in the case of kaon tagging is mainly due to the cross section of nuclear interaction.

	ϵ	ω	ϵ_{eff}	average ϵ_{eff}
$e^\pm$	B^0: 6.32: ± 0.03 % $\overline{B}^0$: 6.21 ± 0.03 %	B^0: 7.4 ± 0.1 % $\overline{B}^0$: 7.4 ± 0.1 %	B^0: 4.59 ± 0.04 % $\overline{B}^0$: 4.50 ± 0.04 %	4.55 ± 0.03 %
$\mu^\pm$	B^0: 6.52 ± 0.03 % $\overline{B}^0$: 6.39 ± 0.03 %	B^0: 8.7 ± 0.1 % $\overline{B}^0$: 8.9 ± 0.1 %	B^0: 4.45 ± 0.04 % $\overline{B}^0$: 4.32 ± 0.04 %	4.38 ± 0.03 %
kaon	B^0: 32.57 ± 0.07 % $\overline{B}^0$: 32.14 ± 0.07 %	B^0: 15.35 ± 0.09 % $\overline{B}^0$: 16.09 ± 0.09 %	B^0: 15.64 ± 0.09 % $\overline{B}^0$: 14.78 ± 0.09 %	15.21 ± 0.06
sum				24.14 ± 0.07%

Table 3.2: ϵ, ω and ϵ_{eff} with high momentum leptons and kaons

3.3 Tagging using leptons with p_l^* and p_{miss}^*

A low primary lepton momentum implies a higher momentum of the accompanying neutrino. The missing momentum in the $\Upsilon(4s)$ rest frame (p_{miss}^*) is a good approximation of the neutrino momentum. Figure 3.5 shows the correlation between p_l^* and p_{miss}^* in neutral B meson

generic events at the generator level. The same plot for other leptons in figure 3.6 shows the clear difference. Therefore by using p_l^* and p_{miss}^* simultaneously, we are able to use the lower momentum leptons. We also expect that this method reduces the wrong tagging fraction with high momentum leptons described in the previous section. We required one and only one lepton in an event which satisfies the following condition;

$$p_l^* > 1.4GeV/c \ \cup \ (p_l^* > 0.6GeV/c \ \cap \ p_l^* + p_{miss}^* > 2.0GeV/c). \tag{3.1}$$

To reconstruct p_{miss}^*, first we calculated the missing momentum in the laboratory system using all the reconstructed particles except for any K_L:

$$\vec{p}_{miss} = \vec{p}_{beam} - \vec{p}_{B_{cp}} - \sum \vec{p}_{charged} - \sum \vec{p}_{\gamma}, \tag{3.2}$$

where for $p_{B_{cp}}$ we used an approximation that B_{cp} was at rest in the center of mass system. Assuming that $\vec{p}_{miss}$ is the momentum of the neutrino, a Lorentz transformation is made to obtain p_{miss}^*. The results are summarized in table 3.3. The total effective efficiency summing e and μ is 10.04±0.04%, which is better than the simple method in the last section by about 1%.

Some attempts for further improvement were carried out, but no sizable gain was obtained. First of all, we considered using the reconstructed momentum of B_{cp} to take into account the finite momentum in the center of mass system. Even if we used the generator information for $\vec{p}_{B_{cp}}$, however, the effective efficiency was improved only by 0.08% for each of $\mu^{\pm}$ and $e^{\pm}$. Therefore the net improvement will be less than 0.16%. We also tried to use the polar angle of the missing momentum in the laboratory frame ($\cos\theta_{\vec{p}_{miss}}$) to avoid the case in which the missing momentum could be due to particles outside the detector acceptance. We required $-0.6 < \cos\theta_{\vec{p}_{miss}} < 0.9$ for muons and electrons with $0.6GeV/c < p_l^* < 0.8GeV/c$. (figure 3.7) This gave a slightly smaller wrong tagging fraction but almost the same effective efficiency as shown in Table 3.3. An attempt to use the recoil mass as another discriminant gave no improvement. Finally we also tried to utilize events with two or more leptons by choosing the one with the highest momentum. The effective efficiency was not improved.

	ϵ	ω	ϵ_{eff}
$e^{\pm}$	7.83±0.03 %	9.5±0.1 %	5.14±0.03 %
$\mu^{\pm}$	7.39±0.03 %	9.4±0.1 %	4.88±0.03 %
$e^{\pm}$ with generator $p_{B_{cp}}$	7.89±0.03 %	9.1±0.1 %	5.28±0.03 %
$\mu^{\pm}$ with generator $p_{B_{cp}}$	7.23±0.03 %	8.7±0.1 %	4.92±0.03 %
$e^{\pm}$ with $\cos\theta_{p_{miss}}$	7.44±0.03 %	8.2±0.1 %	5.19±0.03 %
$\mu^{\pm}$ with $\cos\theta_{p_{miss}}$	7.10±0.03 %	8.6±0.1 %	4.87±0.03 %

Table 3.3: ϵ, ω and ϵ_{eff} for tagging with leptons using p_l^* and p_{miss}^*.

3.4 Tagging with low momentum electrons

We tried to use electrons[3] from decays of charmed hadrons, which are expected to have the opposite charge to leptons from semileptonic B decays. The flavor of B_{tag} can be tagged by

[3] We did not use muons because most of them in the momentum region of interest can not be detected with the KLM.

using the relations $B_{tag} = B^0$ for l^- and $B_{tag} = \overline{B}^0$ for l^+.

Since these electrons have relatively low momenta and these events have low missing momentum, we used the following criteria:

1. Only one electron satisfies the following conditions:
   - $0.3GeV/c < p_l^* < 0.9GeV/c$,
   - $p_l^* + p_{miss}^* < 1.5GeV/c$,
   - The distance between the track and beam axis at the closest approach in $x-y$ plane, $d\rho$, is
     $$d\rho < 0.05cm.$$
   - The distance between the track and the interaction point at the closest approach in z direction, dz, satisfies
     $$dz < 2cm$$
2. No other leptons with $p_l^* > 0.3GeV/c$.

Cuts on $d\rho$ and dz were used to reject electrons from γ conversions. figure 3.8 shows $d\rho$ and dz distributions for electrons.

The result is shown in table3.4. The wrong tagging fraction is large. We investigated the origins of the wrong tagging and found that the main source was electrons from $D_s^{\pm}$ and other charmed mesons such as $D^{\pm}$ and D^0. These charmed mesons are produced by the quark-level decay process $b \to cW^-$ with $W^- \to \overline{c}s$ (and its charge conjugate process).

Since the wrong tagging fraction is larger than that found for flavor tagging with kaons which is 15.72%, this method must be applied after the tagging with kaons. Therefore for practical use the contribution of this method to the effective efficiency will be less than 0.37%.

ϵ	ω	ϵ_{eff}
2.67±0.02%	31.3±0.3%	0.37±0.01%

Table 3.4: Efficiency and wrong tagging fraction for tagging with low momentum electrons.

3.5 Combined tagging

We estimated the effective efficiency with all the methods mentioned in the previous sections.

At first, we tried leptons with p_l^* and p_{miss}^*. If it failed, kaons were used. If tagging with kaons ended unsuccessfully, flavor tagging with low momentum electrons was carried out. The result is shown in table 3.5.

3.6 Summary

The flavor tagging with leptons and kaons was studied with Monte Carlo simulation. The effective efficiency with the simple method using high momentum leptons and the charge sum of kaons is found to be 24.14±0.07% by summing leptons and kaons. By using p_{miss}^*, the

	ϵ	ω	ϵ_{eff}
$e^{\pm}$ with p_l^* and p_{miss}^*	7.83 $\pm$ 0.03%	9.5 $\pm$ 0.1%	5.14 $\pm$ 0.03%
$\mu^{\pm}$ with p_l^* and p_{miss}^*	7.39 $\pm$ 0.03%	9.4$\pm$ 0.1%	4.88 $\pm$ 0.03%
kaons	31.6 $\pm$ 0.05%	15.7 $\pm$ 0.06%	14.81 $\pm$ 0.06%
low p_l^* $e^{\pm}$	1.76 $\pm$ 0.01%	32.5 $\pm$ 0.4%	0.215 $\pm$ 0.009%
sum			25.05 $\pm$ 0.07%

Table 3.5: ϵ, ω and ϵ_{eff} with all the methods combined.

effective efficiency of flavor tagging with leptons is improved by about 1%. Flavor tagging with low momentum electrons was also studied. The wrong tagging fraction of this method is estimated to be 31.3$\pm$0.3%. Due to the large wrong tagging fraction, this method contributed only 0.215$\pm$0.009% to the overall effective efficiency and is found to be not very useful. The overall effective efficiency with leptons and kaons was estimated to be 25.05 $\pm$ 0.07%.

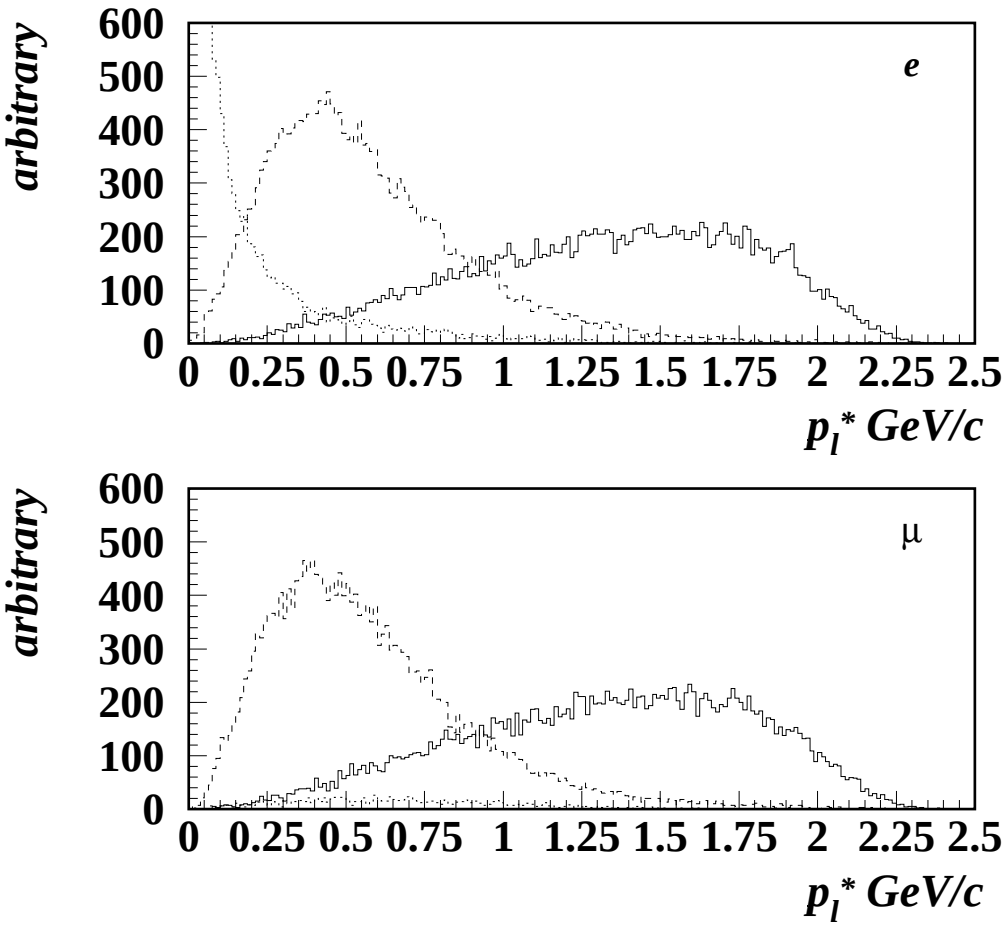

Figure 3.1: The p_l^* distributions for neutral B meson decays at the generator level. The solid histogram is for leptons from B semileptonic decays. The dashed histogram is leptons from cascade charm. The dotted histogram is for other leptons.

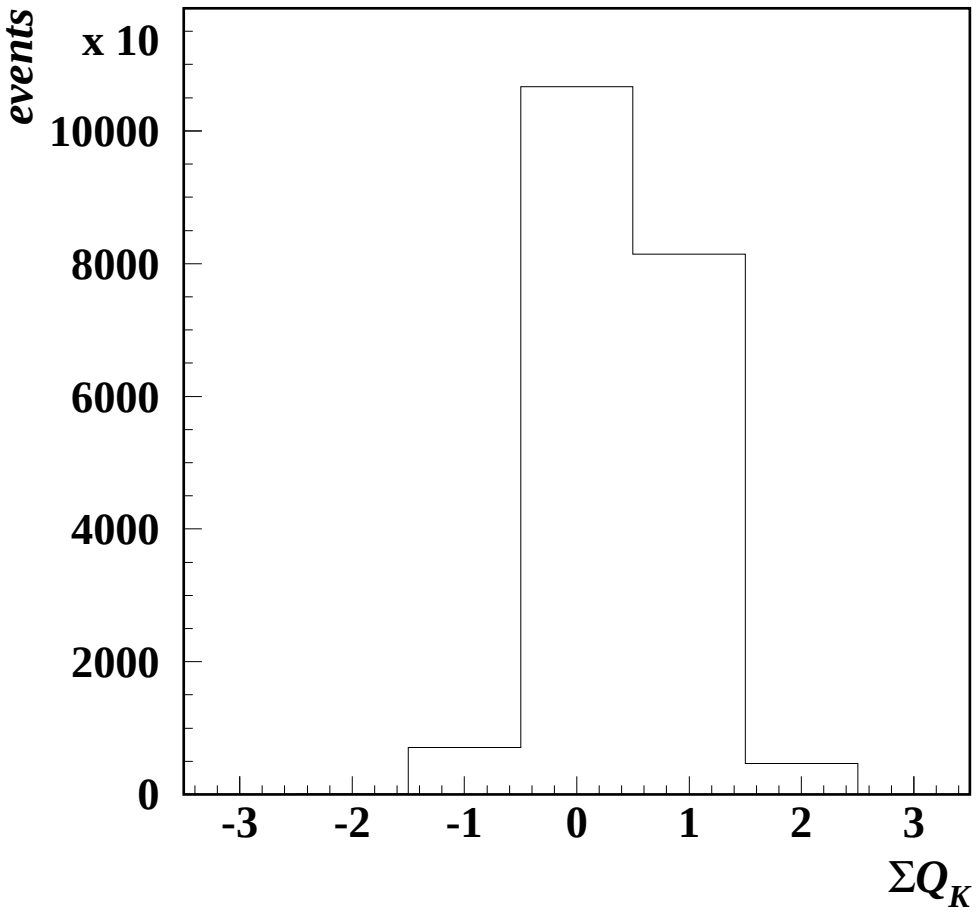

Figure 3.2: Charge sum of charged kaons at the generator level. For events where the B_{tag} flavor is $\overline{B}^0$ the sign of the charge sum is inverted.

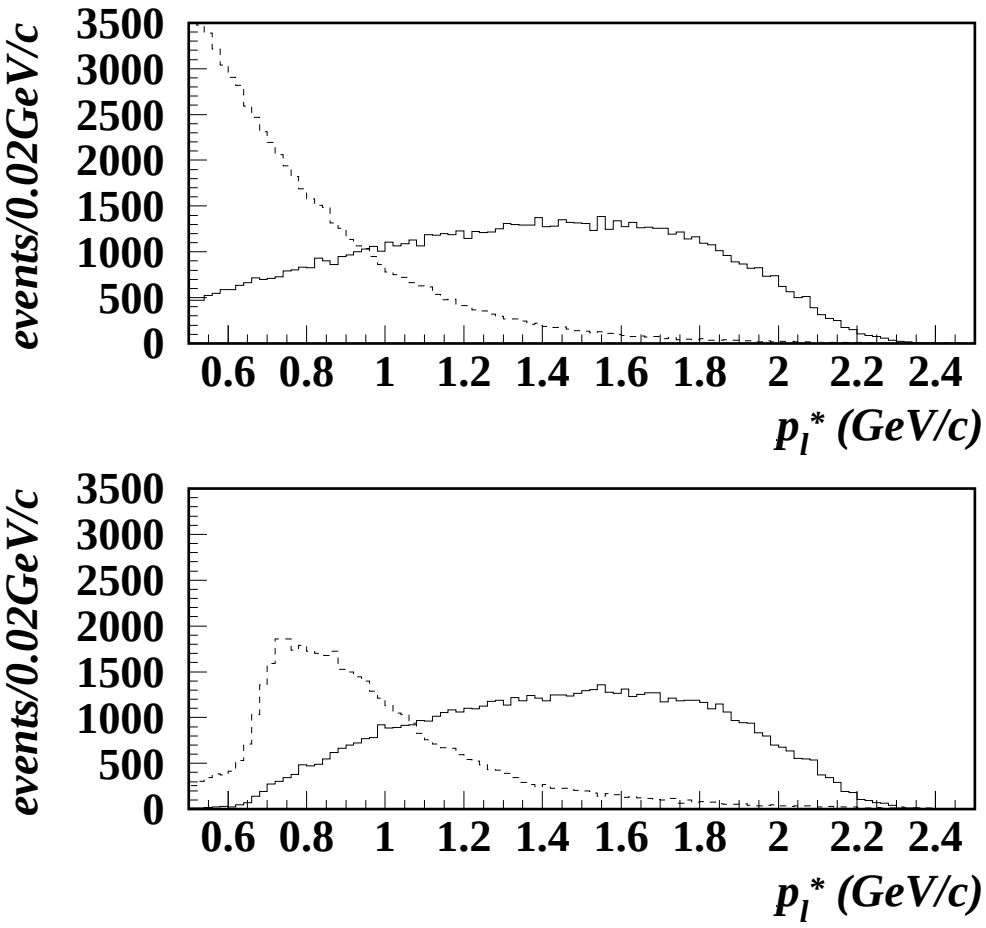

Figure 3.3: Reconstructed p_l^* distributions of electrons (upper figure) and muons (lower figure). The solid histogram is for primary leptons from B semileptonic decays. The dashed histogram is for the other leptons.

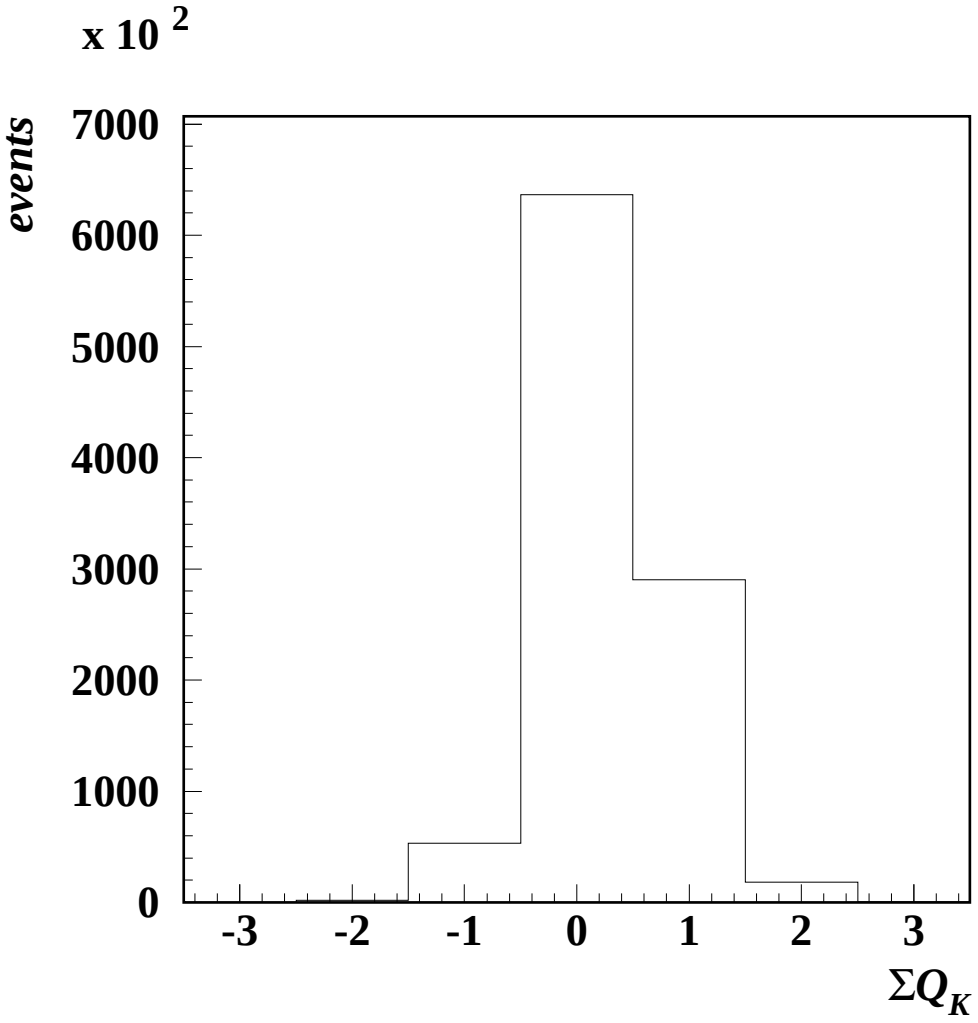

Figure 3.4: Reconstructed kaon charge sum distribution. For events where the true flavor of the B_{tag} is $\overline{B}^0$ the sign of the charge sum is inverted.

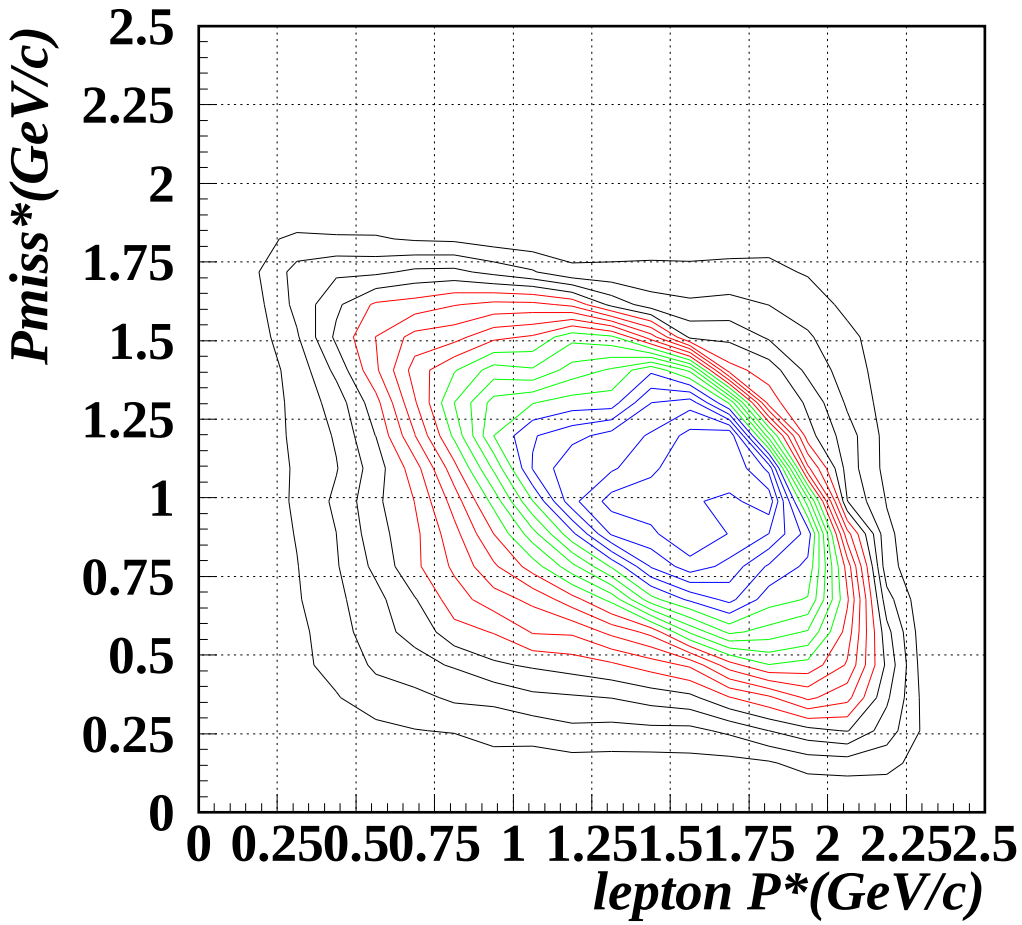

Figure 3.5: P^*_{miss} vs. P^*_l for primary leptons in $B \to l\nu D^{(*)(**)}$ at the generator level

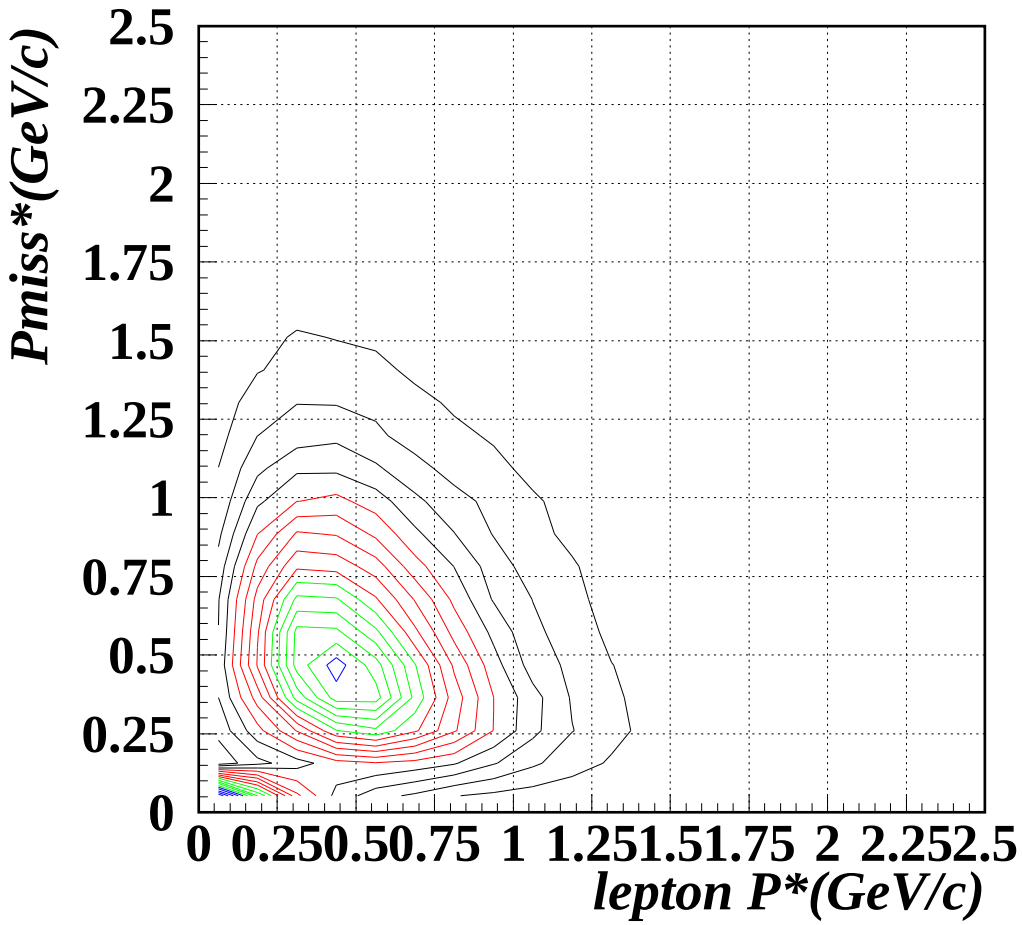

Figure 3.6: P^*_{miss} vs. P^*_l for other leptons at the generator level

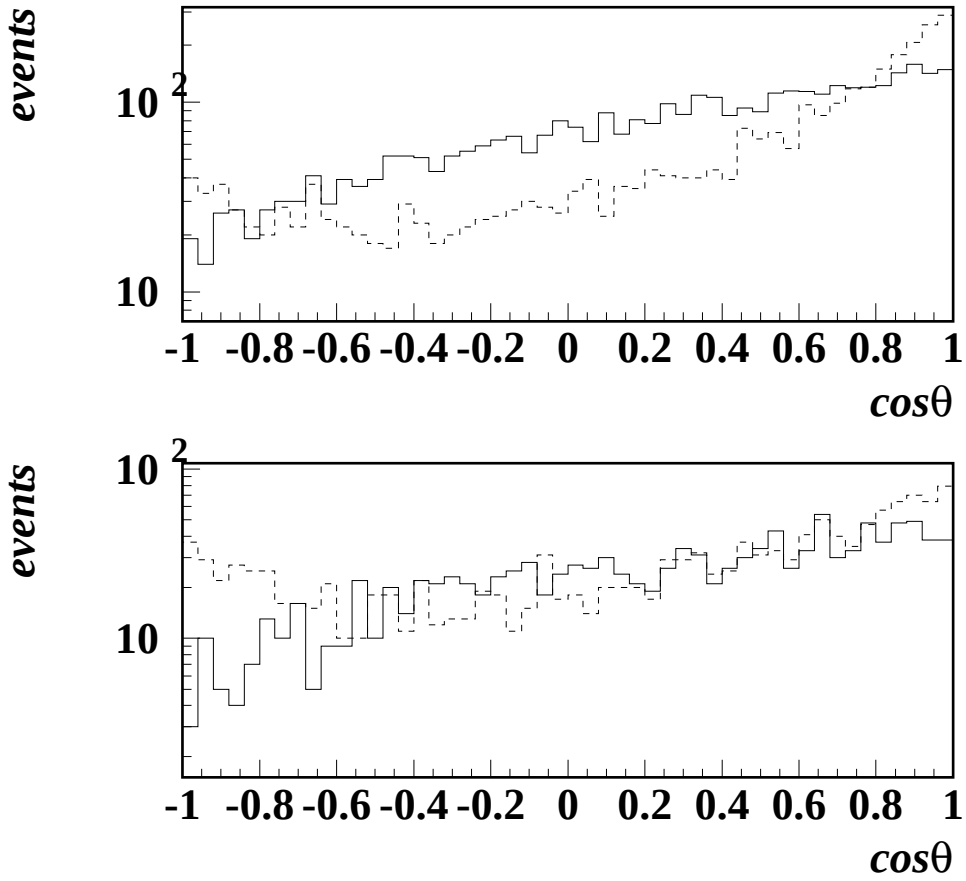

Figure 3.7: $\cos\theta_{P_{miss}}$ distribution of electrons (upper figure) and muons (lower figure) with $0.6GeV/c < p_l^* < 0.8GeV/c$ and $p_l^* + p*_{miss} > 2.0GeV/c$. The solid histogram is for primary leptons from B semileptonic decays. The dashed histogram is for the other leptons.

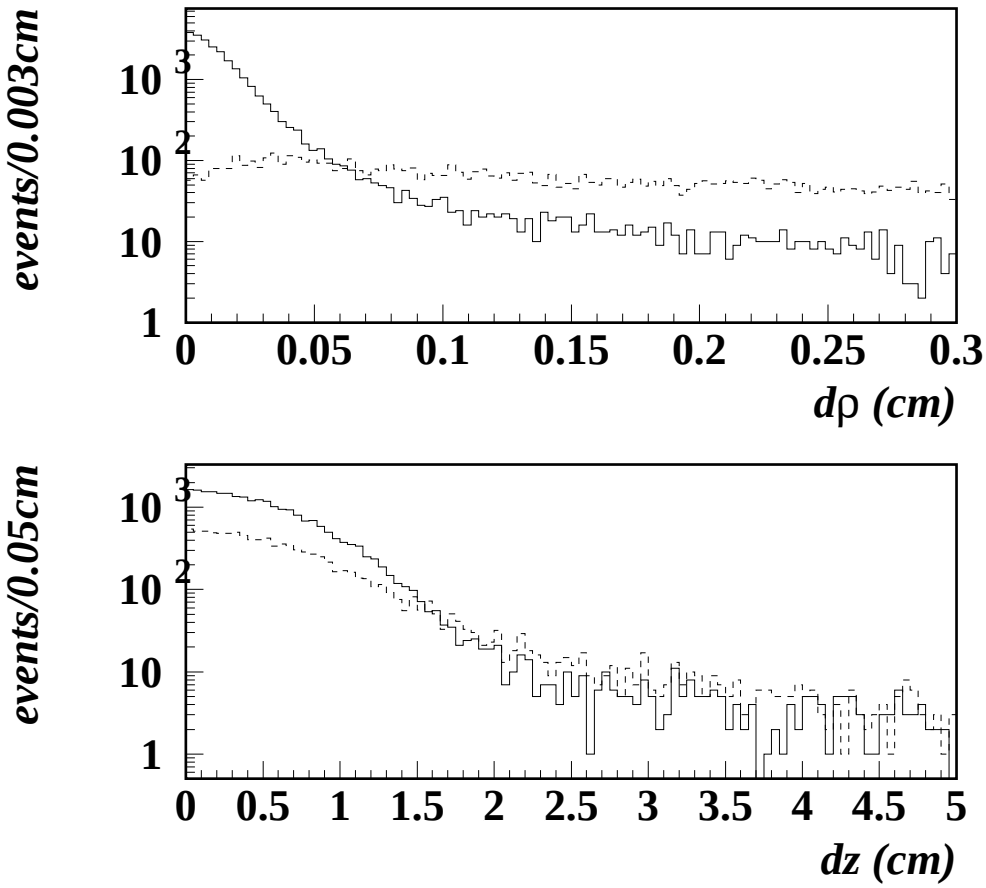

Figure 3.8: $d\rho$ (upper figure) and dz (lower figure) distributions for electrons with $0.3GeV/c < p_l^* < 0.9GeV/c$ and $p_l^* + p_{miss}^* < 1.5GeV/c$. The dashed histogram is for conversion electrons. The solid histogram is for other electrons.

Chapter 4

Flavor tagging performance in real data

In this chapter, we describe the estimation of ω using real data. In section 4.1, we explain how to estimate ω. In section 4.2, we perform a Monte Carlo simulation study to check the validity of our method. In section 4.3, we apply the method to the real data collected with the BELLE detector. In section 4.4, we summarize the result.

4.1 Method

We can estimate ω by using fully reconstructed and flavor specific B mesons in place of B_{cp}. After tagging the flavor of B_{tag} and comparing the flavor of B_{tag} and the flavor specific B meson, the measured ratio ($R_{measured}$) of the number of same-flavor events (N_{sf}) to the number of opposite-flavor events (N_{of}) is given by

$$R_{measured} = \frac{R_{\omega=0} + \omega(1 - R_{\omega=0})}{1 - \omega(1 - R_{\omega=0})}, \tag{4.1}$$

where $R_{\omega=0}$ is obtained with a known mixing parameter $\mathcal{X}_d = 0.172 \pm 0.010$ [8];

$$\begin{aligned} R_{\omega=0} &= \frac{\mathcal{X}_d}{1 - \mathcal{X}_d} \\ &= 0.208 \pm 0.015. \end{aligned} \tag{4.2}$$

From equation (4.1) ω is extracted with the following equation,

$$\omega = \frac{R_{measured} - R_{\omega=0}}{(1 - R_{\omega=0})(R_{measured} + 1)} \tag{4.3}$$

We choose $B^0(\overline{B}^0) \to D^{*-}l^+\nu(D^{*+}l^-\overline{\nu})$ decay as a substitute for B_{cp}, because its branching ratio is large ($\sim 10\%$) and the D^* can be reconstructed cleanly.

4.2 Monte Carlo simulation

We made a study with a Monte Carlo sample to confirm that we can estimate ω with enough accuracy by using this method. We simulated a sample of 8×10^6 $\Upsilon(4S)$ events which corresponded to about 7fb^{-1} of integrated luminosity that will be experimentally achieved in the near future. The mixing parameter in this sample was set to $\mathcal{X}_d = 0.152$.

4.2.1 Preselection

We require the following conditions: [1] .

- The events should have at least three tracks originating from the interaction region.
- The primary event vertex is consistent with the interaction point.
- The total visible energy defined in the center of mass system should be greater than 20% of the center of mass energy.
- The absolute value of the sum of the longitudinal momentum with charged tracks and ECL energy clusters in the rest frame should be less than 50% of the center of mass energy.
- ECL energy sum, (E_{sum}) should be in the range $2.5\% \leq Esum \leq 90\%$ of the center-of-mass energy.

We further require at least one electron or muon which has momentum in the center of mass system greater than $0.5 GeV/c$. We identify muon candidates with the KLM and electron candidates with combined information from the CDC, ACC, TOF and ECL.

4.2.2 $D^0(\overline{D^0})$ reconstruction

By using preselected events, we reconstruct $D^{*\pm}$ through its decays into $D^0(\overline{D^0})\pi^{\pm}$ and $D^0(\overline{D^0})$ into $K^{\mp}\pi^{\pm}$. Hereafter charge conjugation is implied throughout. We identify $K^{\pm}$ candidates with the combined information from the CDC,ACC and TOF. The $K^{\pm}$ candidates are paired with other tracks which have an opposite charge to the kaon candidate. The invariant mass was calculated assuming the nominal mass for each particle:

$$M^2_{K\pi} = \left(\sqrt{M^2_{K^{\pm}} + |\vec{P}_{K^{\pm}}|^2} + \sqrt{M^2_{\pi^{\mp}} + |\vec{P}_{\pi^{\mp}}|^2}\right)^2 - \left|\vec{P}_{K^{\pm}} + \vec{P}_{\pi^{\mp}}\right|^2, \tag{4.4}$$

where $M_{K^{\pm}}$ and $M_{\pi^{\mp}}$ are the nominal mass for the charged kaon and the charged pion respectively. We select D^0 candidates if their invariant mass is within $20 MeV/c^2$ from the D^0 nominal mass. Figure 4.1 shows the M_{K_π} distribution.

4.2.3 $D^{*\pm}$ reconstruction

We combine D^0 candidates with other tracks which have an opposite charge to the kaon in the D^0 candidate. We calculate the invariant mass,

$$M^2_{K\pi\pi} = \left(\sqrt{M^2_{K\pi} + |\vec{p}_{K\pi}|^2} + \sqrt{M^2_{\pi^{\mp}} + |\vec{p}_{\pi^{\mp}{}_s}|^2}\right)^2 - \left|\vec{p}_{K\pi} + \vec{p}_{\pi^{\mp}_s}\right|^2, \tag{4.5}$$

where $\vec{p}_{K\pi}$ is vector sum of momenta of the kaon and the pion in the D^0 candidate, $\vec{p}_{\pi^{\mp}_s}$ is the momentum of the attached pion. We required the mass difference $M_{diff} = M_{K\pi\pi} - M_{K\pi}$ to be in a region:

$$0.1424 GeV/c^2 < M_{diff} < 0.1484 GeV/c^2. \tag{4.6}$$

In addition, the $D^{*\pm}$ momentum ($P^*_{D^{*\pm}}$) in the center of mass system is required to be $P^*_{D^{*\pm}} < 2.5 GeV/c$ so that it is consistent with a daughter particle from B mesons. Figure 4.2 shows the M_{diff} distribution.

[1] We call this HadronA selection.

	N_{sf}	N_{of}
lepton	86	303
kaon	241	679
sum	327	982

Table 4.1: The number of flavor tagged events.

4.2.4 $D^{*\pm}l^{\mp}\nu$ reconstruction

Finally, $D^{*\pm}$ candidates are combined with $\mu^{\mp}$ or $e^{\mp}$ candidates which have opposite charge to the $D^{*\pm}$. Lepton candidates are required to have momentum in the center of mass system (p_l^*) within the range $1.4GeV/c < p_l^* < 2.5GeV/c$.

To utilize the approximately massless characteristic of the ν, we calculate the following two values in the center of mass system,

$$MM^2 = (E_B - E_{D^*l})^2 - |\vec{p}_B|^2 - |\vec{p}_{D*l}|^2 \tag{4.7}$$

$$C = 2|\vec{p}_B||\vec{p}_{D*l}| \tag{4.8}$$

where E_B and $|\vec{p}_B|$ are the energy and momentum of the B meson in the center of mass system, respectively. MM^2 is the measured missing mass squared. E_B and $|\vec{p}_B|$ are calculated from the beam energy and nominal B meson mass,

$$\begin{aligned} E_B &= 5.29GeV/c^2 \\ |\vec{p_B}| &= \sqrt{E_B^2 - M_B^2} = 325MeV/c \end{aligned} \tag{4.9}$$

E_{D^*l} and $|\vec{p}_{D^*l}|$ are the sum of the energy and momenta of the $D^{*\pm}$ candidate and lepton candidate in the center of mass system. These two quantities are related to the mass of the accompanying ν as,

$$M_\nu = MM^2 + C\cos\Theta_{p_B p_{D^*l}} \tag{4.10}$$

where $\Theta_{p_B p^*_D l}$ is the angle between $\vec{p}_B$ and $\vec{p}_{D^*l}$. Since $\Theta_{p_B p_{D^*l}}$ can not be measured and $\cos\Theta_{p_B p^*_D l}$ takes a value ranging between -1 and 1, equation (4.10) leads to the following relation,

$$C \geq |MM^2|. \tag{4.11}$$

We select $D^{*\pm}l^{\mp}\nu$ candidates satisfying this relation. Figure 4.3 shows C vs. MM^2 distribution. After all the cuts mentioned above 2948 events remained.

4.2.5 Flavor tagging

We perform flavor tagging for the tagging side (B_{tag}) of the reconstructed $D^{*\pm}l^{\mp}\nu$ candidate events using a high momentum lepton and charge sum of kaons. The results are shown in Table 4.1. As these numbers include the contribution of background, we need to estimate and subtract them.

4.2.6 Background estimation

Background events for $D^{*\pm}l^{\mp}\nu$ decay mode are divided into four categories:

- Combinatoric background in $D^{*\pm}$ reconstruction.
- Uncorrelated $D^{*\pm}$-lepton background. In this class of events the $D^{*\pm}$ and lepton come from different B mesons.
- Correlated $D^{*\pm}$-lepton background. In this case $D^{*\pm}$ and lepton have the same parent that can be either a neutral or charged B.
- Lepton fakes and continuum events

$D^{*\pm}$ combinatoric background

This type of background is further divided into two types. One is the combination of random $K^{\mp}\pi^{\pm}$ pairs and any pion including pions from real $D^{*\pm}$. The other is the combination of a correctly reconstructed D^0 and a random charged pion. We call the former type of background $K\pi$ combinatoric and the latter $D^0\pi$ combinatoric.

The $M_{K\pi}$ distribution of $K\pi$ combinatoric background does not peak at the mass of D^0 meson. We fitted $M_{K\pi}$ distributions of events without flavor tagging with a Gaussian signal plus linear background. The ratio of the number of the background events in the signal region to the upper sideband region is calculated. We define the sideband region as $1.965GeV/c^2 < M_{K\pi} < 2.065GeV/c^2$. The distribution is shown in figure 4.4. We obtained 1.11 ± 0.09 as the ratio. We count the number of events in the upper sideband region and scale it with this ratio to estimate this type of background.

The $D^0\pi$ type of background does not have a peak in the M_{diff} distribution, but peaks at the mass of the D^0 meson. We use the M_{diff} upper sideband region to estimate this type of background. We use $0.16GeV/c^2 < M_{diff} < 0.19GeV/c^2$ as this region. We count the number of events in this M_{diff} region and subtract the $K\pi$ combinatoric background using the same method we mentioned above. After that, the number of remaining events is scaled to the M_{diff} signal region and subtracted as this type of background. The scaling factor is determined by fitting the M_{diff} distribution of events without flavor tagging . Since the M_{diff} distribution has a have long tail toward the higher M_{diff} region, we fit the sideband region with the background function, $a(M_{diff} - M_{\pi})^{\frac{1}{2}} + b(M_{diff} - M_{\pi})^{\frac{3}{2}}$ where a and b are free parameters, and extend it into the signal region. We obtained 0.112 ± 0.006 as the scaling factor.

Uncorrelated D^*-lepton background

Since the uncorrelated D^*-lepton background can have more energy than one B decay, their MM^2 can have a smaller value than the signal and correlated background. We use the $C < 0.8|MM^2|$ and $MM^2 < 0$ region to estimate this type of background. Except for combinatoric background, the events in this region are expected to be almost pure uncorrelated events. We count the number of events in this region and subtract the combinatoric background using the same method mentioned above. After that, the remaining number is scaled to the signal region. The scaling factor is determined with an independent Monte Carlo study to be $= 0.24 \pm 0.05$.

	signal region	D^* combinatoric	*Uncorrelated*	*Correlated*	BG subtracted
Without tagging	2948	392 ± 23	61 ± 15	190 ± 55	2304 ± 86
Lepton SF	86	7 ± 2	9 ± 3	7 ± 5	62 ± 11
Lepton OF	303	23 ± 4	3 ± 1	33 ± 8	244 ± 21
Kaon SF	241	43 ± 6	8 ± 3	15 ± 13	175 ± 22
Kaon OF	679	73 ± 7	7 ± 3	43 ± 15	556 ± 32
SF sum	327	51 ± 6	18 ± 5	22 ± 14	237 ± 25
OF sum	982	96 ± 8	10 ± 3	76 ± 18	800 ± 39

Table 4.2: The estimated numbers of background events.

Correlated $D^{*\pm}$-lepton background

The correlated $D^{*\pm}$-lepton background comes from the decay of a charged or neutral B meson into $D^{*\pm}l^{\mp}\nu + anything$. Therefore they tend to have a larger MM^2 value than that of the signal. We use the $C < 0.8|MM^2|$ and $MM^2 > 0$ region to estimate this background. We count the number of events in this region and subtract combinatoric background with the same method mentioned above. The uncorrelated background in this region is also subtracted by scaling the number of uncorrelated events with $C < 0.8|MM^2|$ and $MM^2 < 0$ with the factor 0.11 ± 0.04 determined with an independent Monte Carlo study. Since this region has non-negligible leakage of signal compared with the correlated background in this region, we calculate the number of this type of background events in the signal region by solving the following simultaneous equations,

$$\begin{cases} N_{\text{sig. region}} = N_{signal} + r_C N_{BG} \\ N_{\text{cor. region}} = r_S N_{signal} + N_{BG} \end{cases} \tag{4.12}$$

where $N_{\text{sig. region}}$ and $N_{\text{cor. region}}$ denote the number of events in the signal region and the $C < 0.8|MM^2|$ and $|MM^2| > 0$ region, respectively. N_{signal} and N_{BG} is the number of $D^*l\nu$ signal events in the signal region and correlated background events in the $C < 0.8|MM^2|$ and $|MM^2 > 0$ region,respectively. The ratio r_S is the quotient of the number of $D^*l\nu$ signal events in the $C < 0.8|MM^2|$ and $|MM^2| > 0$ region divided by that in the signal region The ratio r_C is a quotient of the number of correlated background events in the signal region divided by that in the $C < 0.8|MM^2|$ and $|MM^2| > 0$ region. The ratios $r_S = 0.010 \pm 0.003$ and $r_C = 1.26 \pm 0.2$ were estimated with an independent Monte Carlo sample.

Lepton fakes and continuum

Lepton fakes are rare enough to be neglected thanks to the good particle identification capability of BELLE. Continuum events were also studied with 10^7 Monte Carlo events that correspond to 3.6fb^{-1}. The background level is only 3%.

The estimated numbers of background events is shown in Table 4.2.

4.2.7 Result

We estimate flavor tagging performance with BG-subtracted signal listed in the rightmost column of table 4.2. The result is given in table 4.3. The error does not include the error of the

	ϵ	ω	ϵ_{eff}
Lepton	13.3 ± 1.1 %	7.3 ± 4.6 %	9.7 ± 2.2 %
Kaon	31.7 ± 2.1 %	12.6 ± 3.6 %	17.8 ± 3.6
Sum	45.0 ± 2.6 %	11.0 ± 2.9 %	27.3 ± 4.4 %

Table 4.3: The estimated tagging performance with $D^{*\pm}l^{\mp}\nu$ events from 8×10^6 $\Upsilon(4S)$ Monte Carlo Sample.

	ω
Lepton	7.3 ± 4.6 ± 1.1 %
Kaon	12.6 ± 3.6 ± 1.0 %
Sum	11.0 ± 2.9 ± 1.0 %

Table 4.4: ω considering 6% uncertainty of the mixing parameter. The second error is due to the uncertainty of mixing parameter.

mixing parameter. Considering the 6% error of the mixing parameter, the error of ω is given in table 4.4.

This result is consistent with the performance estimated in the chapter 3 (table 3.2).

4.2.8 Discussion

As we mentioned in section 1.5, the uncertainty in ω gives a systematic error for the CP violation measurement. This error should be smaller than statistical error of the CP violation measurement. According to a Monte Carlo study of the sensitivity to the CP asymmetry with 100fb^{-1} integrated luminosity[10] the corresponding statistical error of the CP asymmetry is about 13%. From table 4.4, the error in the CP asymmetry due to the error of ω for 7fb^{-1} is,

$$\frac{\delta a_{f_{CP}}}{a_{f_{CP}}} = \frac{\delta(1-2\omega)}{(1-2w)} = 0.08 \tag{4.13}$$

in the case of using lepton and kaon tagging. The error is already smaller than the statistical error with 100fb^{-1}. Therefore we conclude this method can estimate ω with enough accuracy for the CP violation measurement. If we scale our result to 100fb^{-1}, the error of ω becomes ± 0.8 ± 1.0 %, and the contribution to the error of the CP asymmetry becomes 3%.

4.3 ω estimation with real data

In this section, we apply our method to the real data. We use the data collected with the BELLE detector in the autumn of 1999. The data corresponds to an integrated luminosity of 235.1pb^{-1} on the $\Upsilon(4S)$ resonance.

without tag	61
lepton SF	2
lepton OS	7
kaon SF	5
kaon OF	12
tagged sum SF	7
tagged sum OF	19

Table 4.5: The number of events after all the cuts.

4.3.1 Event selection

We apply the event selection criteria which are basically identical to that in the previous section. The $M_{K\pi}$ signal region is shifted to $1.841 GeV/c^2 < M_{K\pi} < 1.881 GeV/c^2$, since the peak position of real data shifts lower due to our imperfect momentum calibration. In addition, we require the ratio of the second to the zeroth Fox Wolfram moments [9] calculated with charged tracks to be less than 0.6 to suppress non-hadronic background. From Monte Carlo simulation, the loss of signal $D^{*\pm}l^{\mp}\nu$ events due to this additional cut is estimated to be less than 1% and is negligible.

Figure 4.6 shows the $M_{K\pi}$ distribution in the preselected data. Figure 4.7 shows the M_{diff} distribution after the cut on $M_{K\pi}$ and on $p^*_{D^*}$. The C vs. MM^2 distribution after all the cuts except for that on C vs. MM^2 is shown in figure 4.8.

After flavor tagging, we obtained the number of events listed in table 4.5.

4.3.2 Background estimation

Since the statistics is very small, we did not use the same procedure as that used for Monte Carlo sample.

First we estimate the number of background events in the signal region without flavor tagging.

The $M_{K\pi}$ distribution of the events which pass all the cuts except for the $M_{K\pi}$ cut and flavor tagging is shown in figure 4.9. The clear D^0 peak is seen and the background in the sideband region is small. Therefore we neglect random $K\pi$ combinatoric background.

The remaining combinatoric background is due to random combinations of correctly reconstructed D^0 or $\overline{D^0}$ and pions. The M_{diff} distribution of the events which pass all the cuts except for the M_{diff} cut and flavor tagging is shown in figure 4.10. We can see a clear peak of the $D^{*\pm}$ signal and there are some background events. We count the number of events in the $0.16 GeV/c^2 < M_{diff} < 0.19 GeV/c^2$ region and subtract $K\pi$ combinatoric background scaling the number of events in the upper sideband region $1.965 GeV/c^2 < M_{K\pi} < 2.065 GeV/c^2$ with the ratio of the area of the signal region to the sideband region (figure 4.11). After that, the remaining $D^0(\overline{D^0})$ signals in the M_{diff} sideband region is scaled with the ratio of the area of the signal region to the sideband region.

For uncorrelated backgrounds, we count the number of events in the $C < 0.8|MM^2|$ and $|MM^2| < 0$ region and obtain 15 events. The $M_{K\pi}$ and M_{diff} distributions are shown in figure 4.12 and figure 4.13, respectively. We can see the 15 events including some combinatoric backgrounds and there are a few excess events in signal region. Since the uncorrelated background is scaled to the signal region with the ratio of about 0.24 mentioned in section 4.2.6, the number is

	signal region	background	BG subtracted
without tagging	61	11 ± 4	50 ± 9
lepton SF	2	negligible	2 ± 1
lepton OF	7	negligible	7 ± 3
kaon SF	5	1 ± 2	4 ± 3
kaon of	12	2 ± 2	10 ± 4
SF sum	7	1 ± 2	6 ± 3
OF sum	19	2 ± 2	17 ± 5

Table 4.6: The estimated numbers of background for real data.

	ϵ	ω	ϵ_{eff}
lepton	18 ± 7 %	8 ± 17 %	13 ± 12 %
kaon	28 ± 11 %	17 ± 26 %	12 ± 20 %
sum	46 ± 14 %	14 ± 17 %	24 ± 24 %

Table 4.7: Estimated performance of flavor tagging for real data.

smaller than 3.6 and is negligible compared with the statistical error of the events in the signal region which is 8.

For correlated background, the number of events in the region $C < 0.8 \times MM^2$ is 6. The $M_{K\pi}$ and M_{diff} distributions in this region are shown in figure 4.14 and 4.15. There is no clear excess in the signal region and they are consistent with combinatoric background. Therefore we neglect the correlated background.

For flavor tagged events, we estimated only the combinatoric background which is the random combination of correctly reconstructed $D^0(\overline{D^0})$ and pions, because other backgrounds are negligible as we already mentioned. The $D^{*\pm}$ combinatoric background is estimated with the M_{diff} sideband. We counted the number of events in the $0.16 < M_{K\pi} < 0.19$ region and subtract the combinatoric $K\pi$ background in this region and scale it with the ratio of the area of the signal region to the sideband region, as mentioned in this section.

The estimated numbers of background events are shown in table 4.6.

4.3.3 Result

The estimated tagging performance for the real data is shown in table 4.7. The error is quite large due to small statistics. We cannot say anything conclusive, but this is consistent with the Monte Carlo expectation shown in table 3.2.

We calculated the branching ratio of $B^0(\overline{B}^0) \to D^{*-}l^+\nu(D^{*+}l^-\overline{\nu})$ as a cross-check to confirm that we reconstructed $D^{*\pm}l^{\mp}\nu$ properly. The efficiency of the reconstruction is estimated to be $10.3 \pm 0.2\%$ with Monte Carlo simulation. The branching ratio for $D^{*\pm} \to D^0(\overline{D^0})\pi^{*\pm}$ and $D^0(\overline{D^0}) \to K^{\mp}\pi^{\pm}$ is 68.3 ± 1.4 and $3.85 \pm 0.09\%$ [8], respectively. The production cross section of $\Upsilon(4S)$ is 1.15nb [11]. We assume the branching ratio of $\Upsilon(4S) \to B^0\overline{B}^0$ is 0.5. The branching

ratio BR($B^0(\overline{B}^0) \to D^{*\pm} l^{\mp} \nu$) is given by,

$$\mathrm{BR}(B^0(\overline{B}^0) \to D^{*\pm} l^{\mp} \nu) = \frac{50}{0.103 \times 0.0383 \times 0.683} \times \frac{1}{235.1\mathrm{pb}^{-1} \times 1.15\mathrm{nb} \times 0.5 \times 2} = 6.9 \pm 1.2\% \tag{4.14}$$

where error is statistical only. This is consistent with the known value of $9.20 \pm 0.54\%$ [8].

4.4 Summary

Performance of the flavor tagging with real data was studied. From Monte Carlo study, it is found that we can estimate ω with enough accuracy for the CP violation measurement by using $B^0(\overline{B}^0) \to D^{*\mp} l^{\pm} \nu$ decays in place of B_{cp}.

We also applied the method to the real data collected with the BELLE detector. Statistics is limited but the performance of the flavor tagging is consistent with Monte Carlo expectation. We checked the validity of our reconstruction method for $B^0(\overline{B}^0) \to D^{*\mp} l^{\pm} \nu$ decays by calculating the branching ratio from the number of reconstructed events with real data. We found that the estimated branching ratio was consistent with the known value and confirm that we reconstructed $B^0(\overline{B}^0) \to D^{*\mp} l^{\pm} \nu$ decay properly.

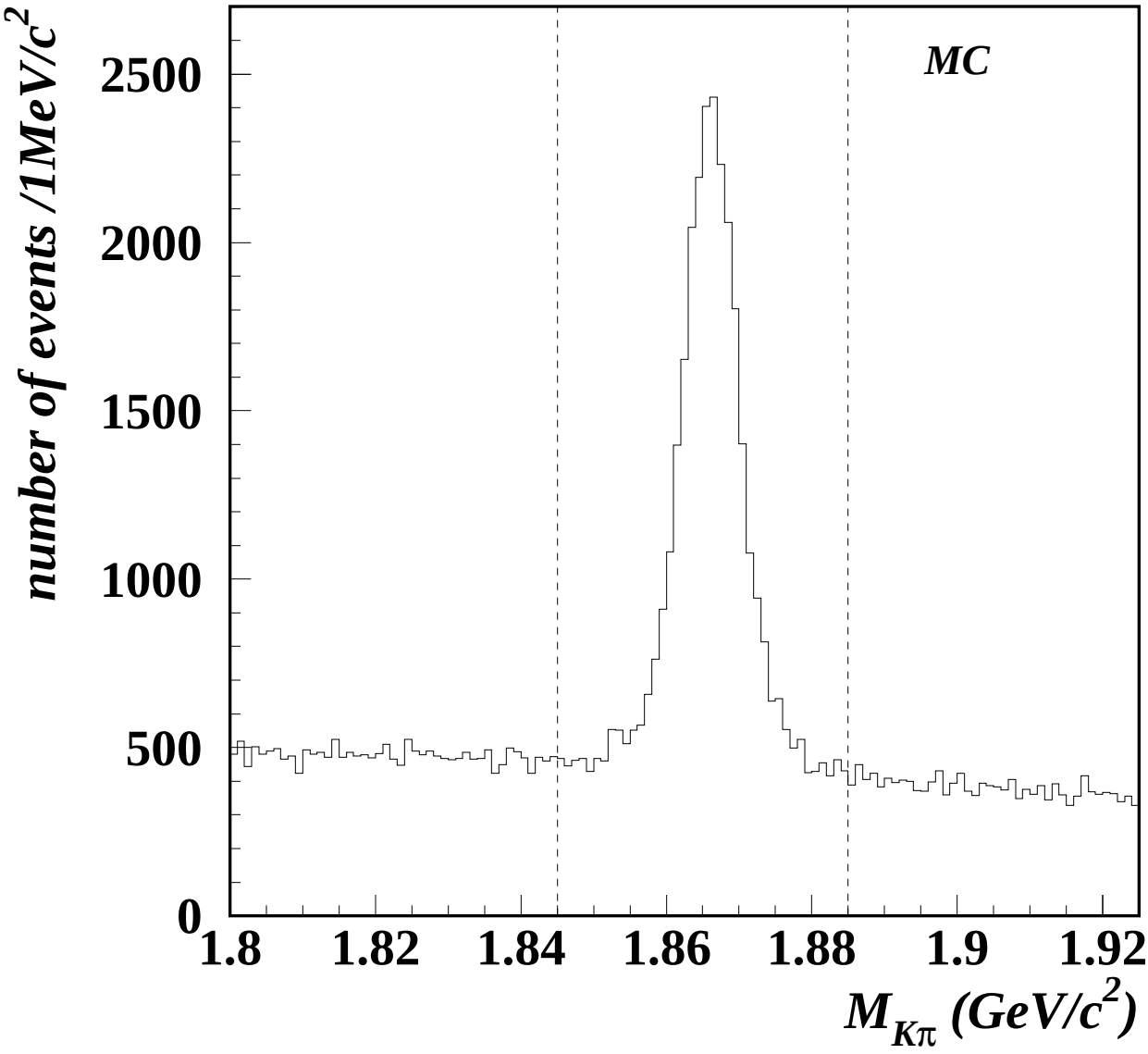

Figure 4.1: $M_{K\pi}$ distribution in the Monte Carlo sample. Dashed lines show signal region.

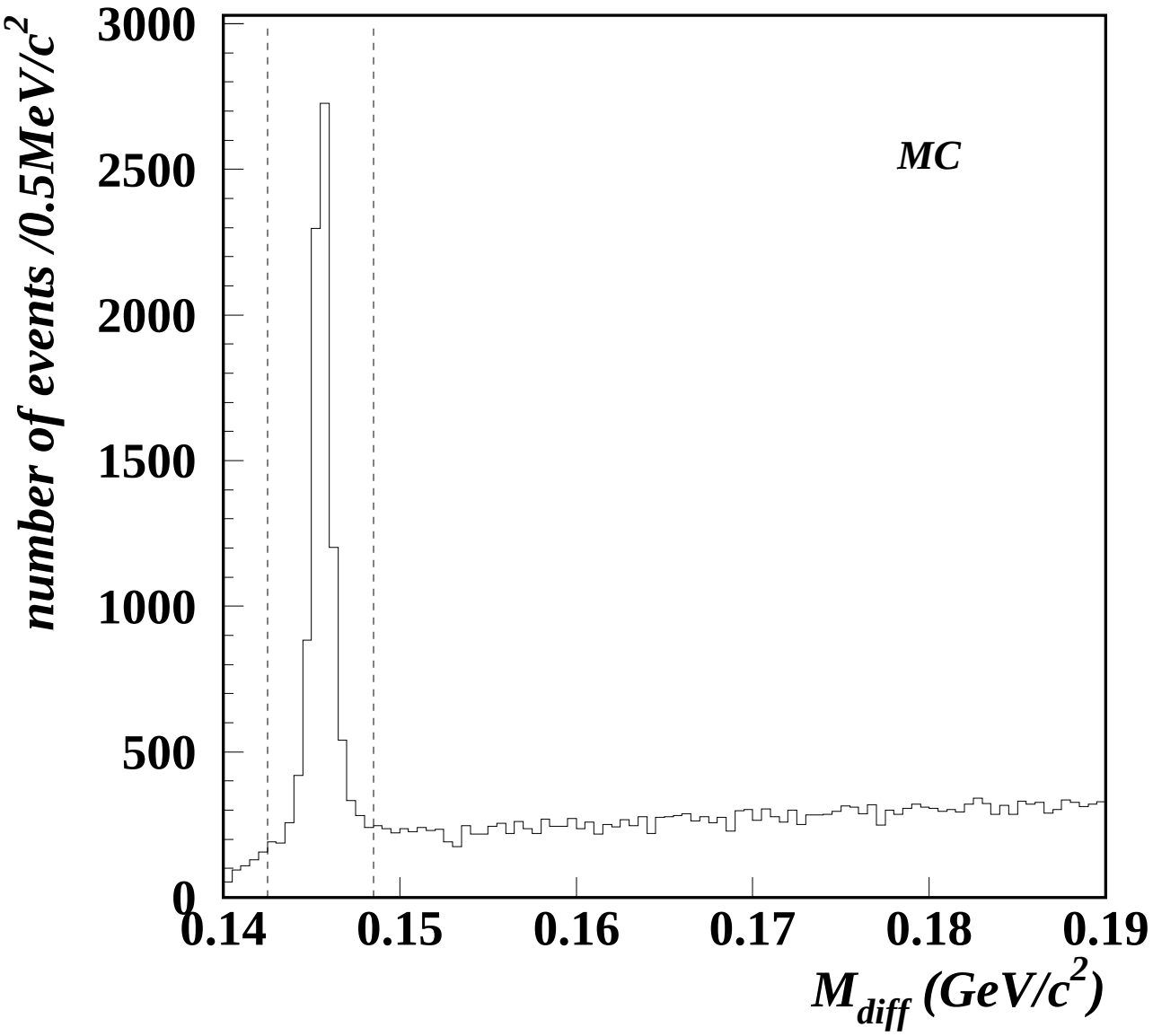

Figure 4.2: Distribution of M_{diff} for the Monte Carlo sample after the $M_{K\pi}$ cut. Dashed lines show signal region.

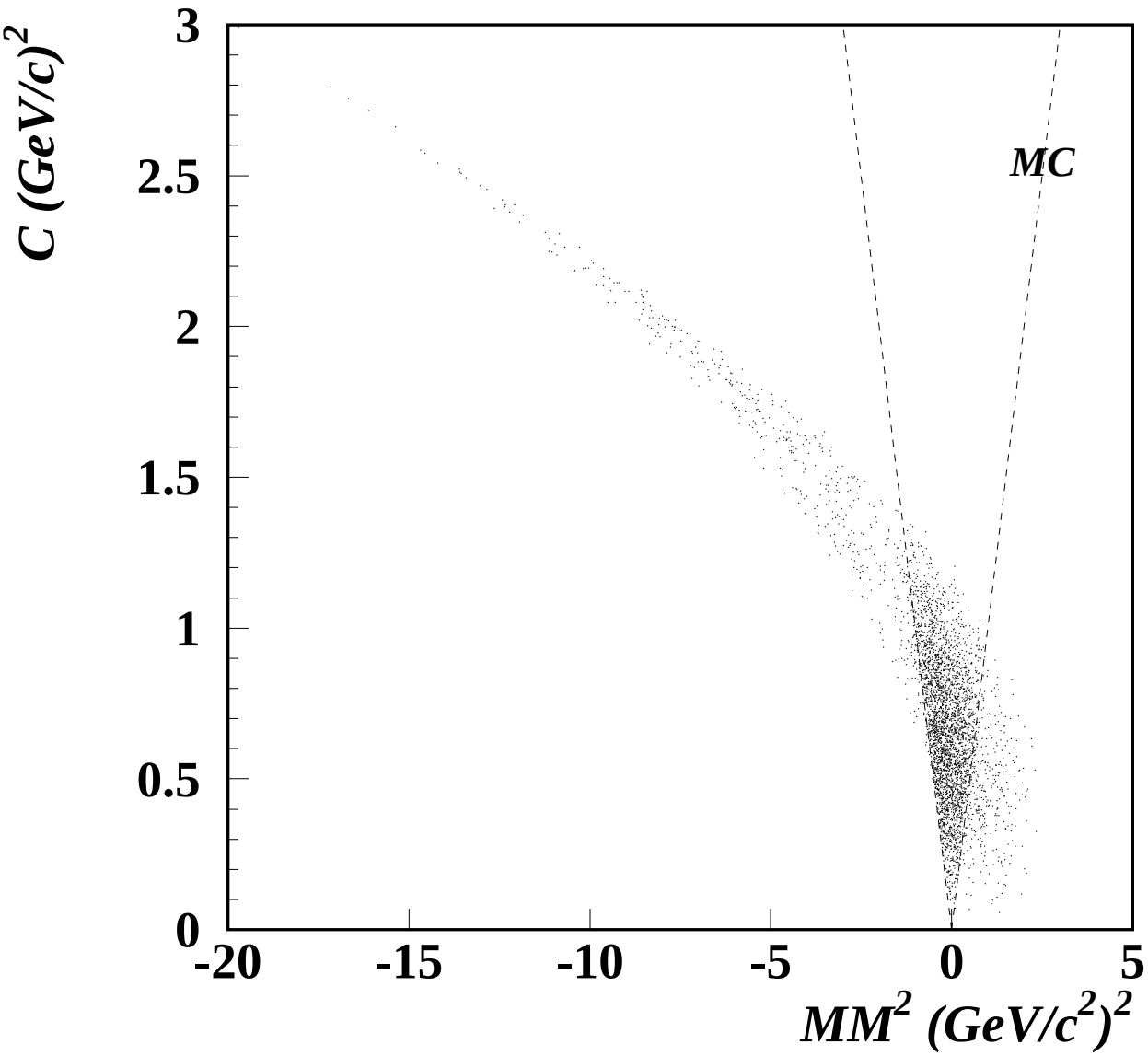

Figure 4.3: C vs. MM^2 distribution for the Monte Carlo sample after all the cuts except for C vs. MM^2. The space between Dashed lines shows the signal region.

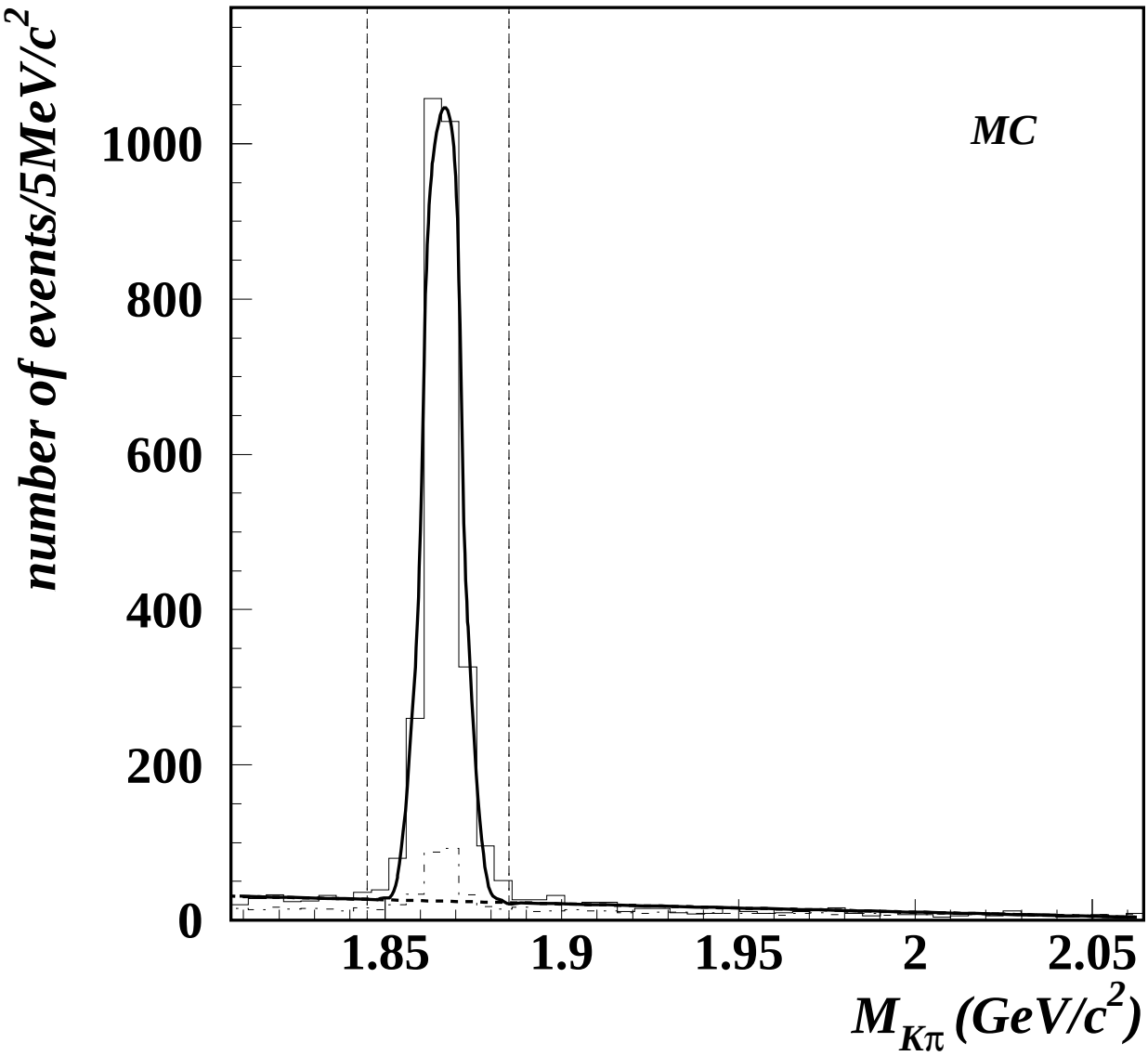

Figure 4.4: $M_{K\pi}$ distribution for the Monte Carlo sample after cuts. Solid histogram is the distribution. Solid line shows the fit with a Gaussian signal plus linear background. Thick dashed line shows background function. Overlaid dot-dashed histogram is scaled M_{diff} sideband. Vertical dashed line shows the signal region.

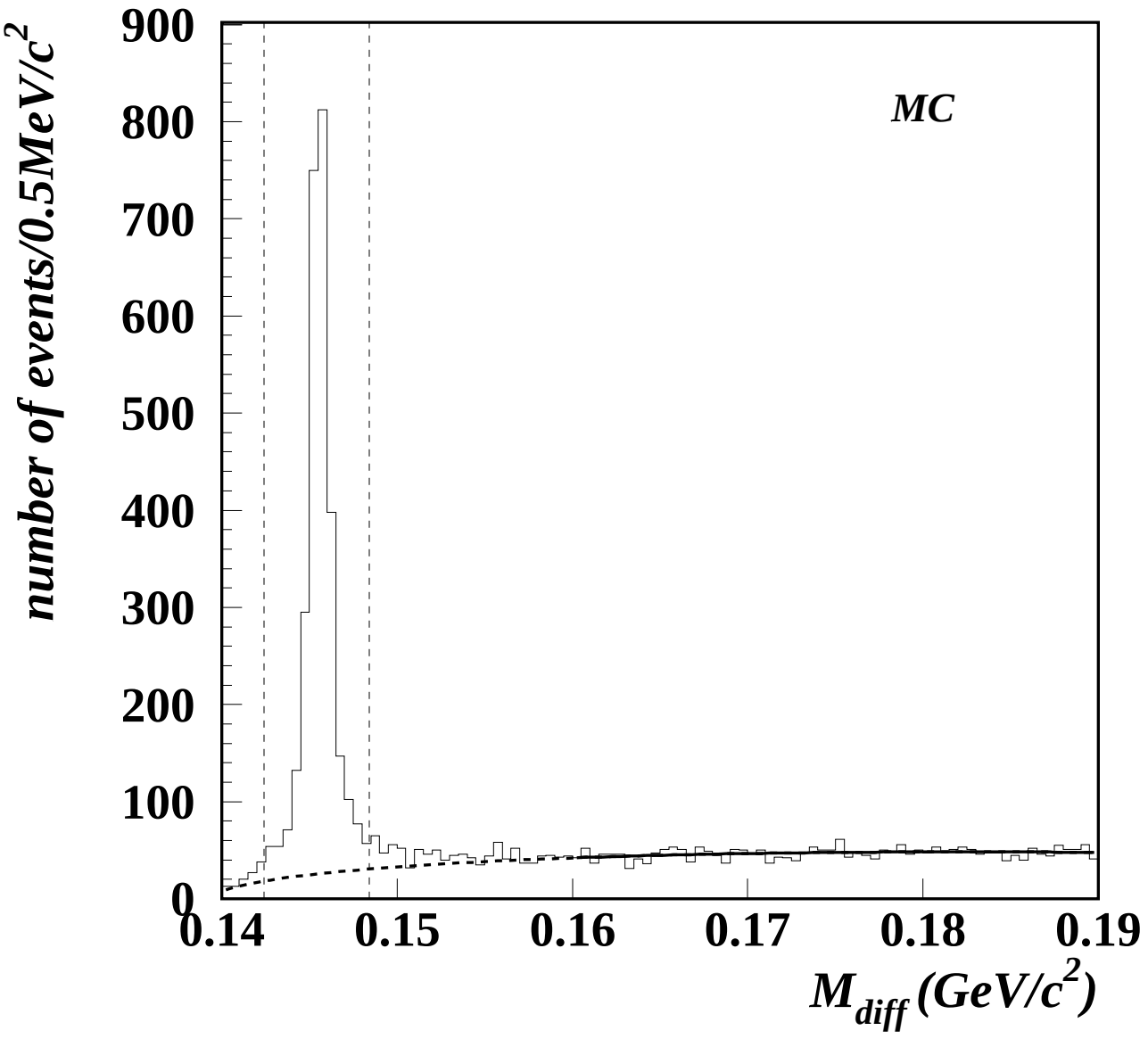

Figure 4.5: M_{diff} distribution for the Monte Carlo sample after cuts. Solid line is the fit with the background function. Thick dashed line shows extended background function. Thin dashed line shows the signal region.

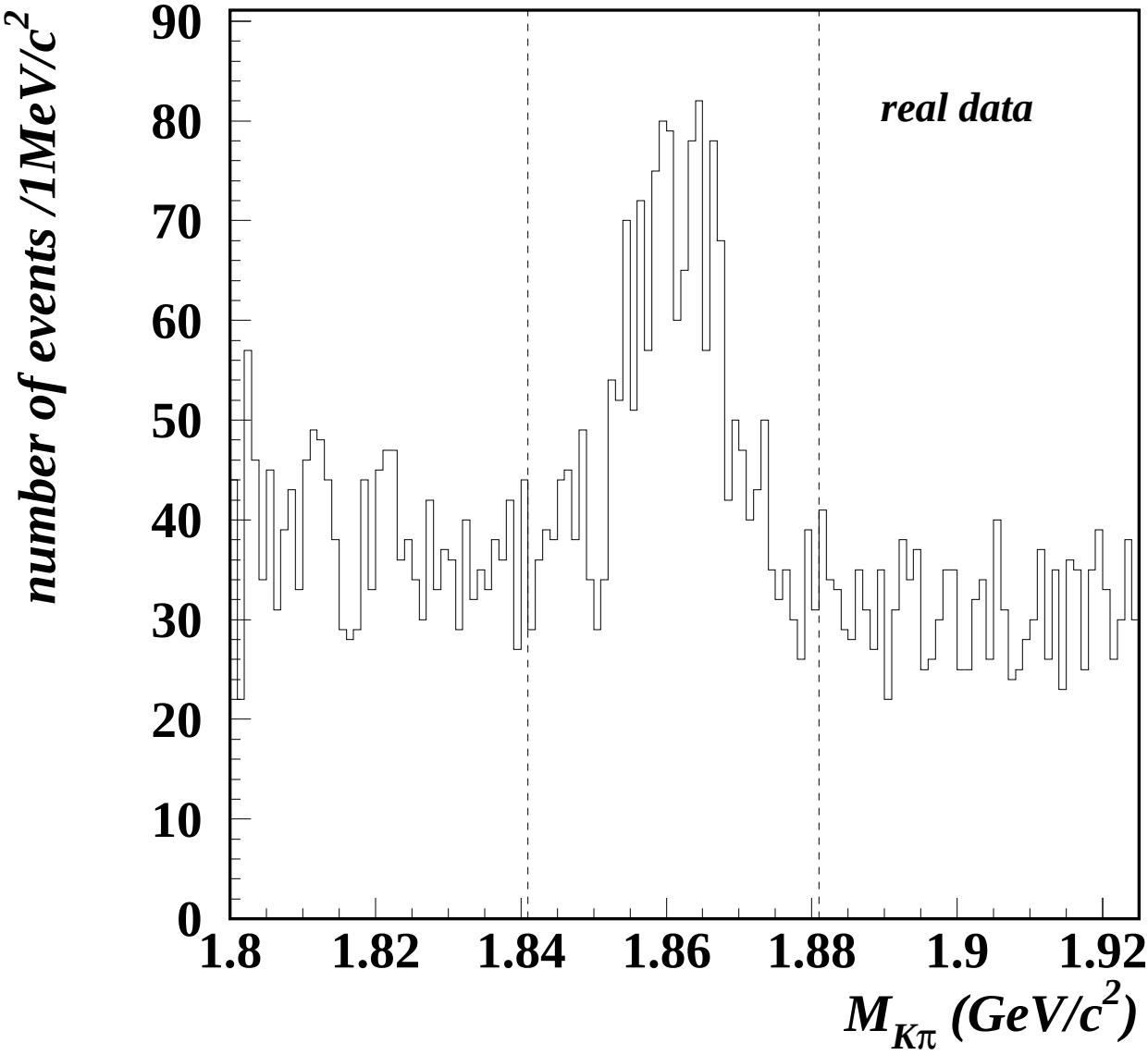

Figure 4.6: Distribution of $M_{K\pi}$ for real data. Dashed lines show the signal region.

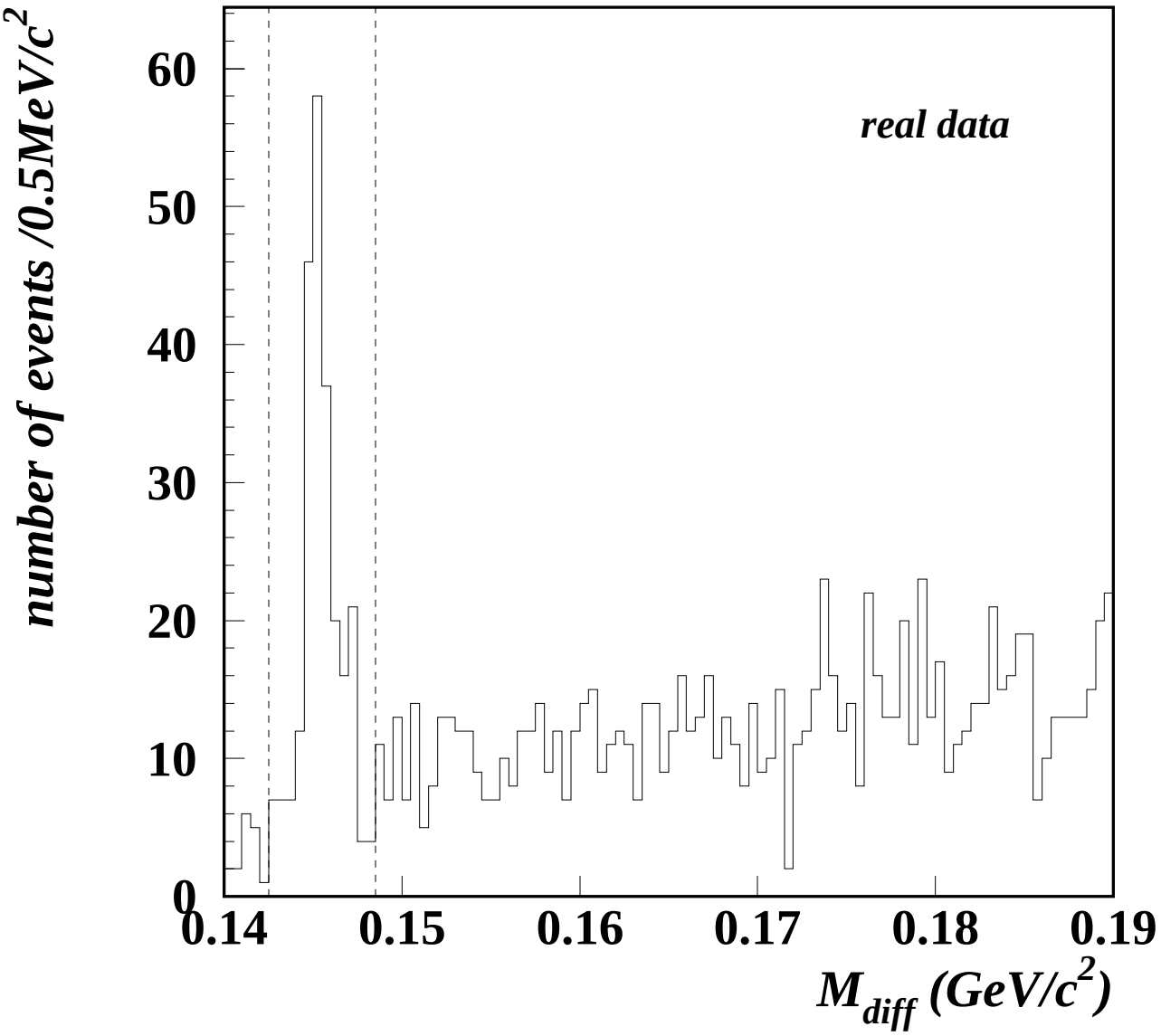

Figure 4.7: Distribution of M_{diff} for real data events which pass the cut on $M_{K\pi}$ and $p^*_{D^*}$. Dashed lines show the signal region.

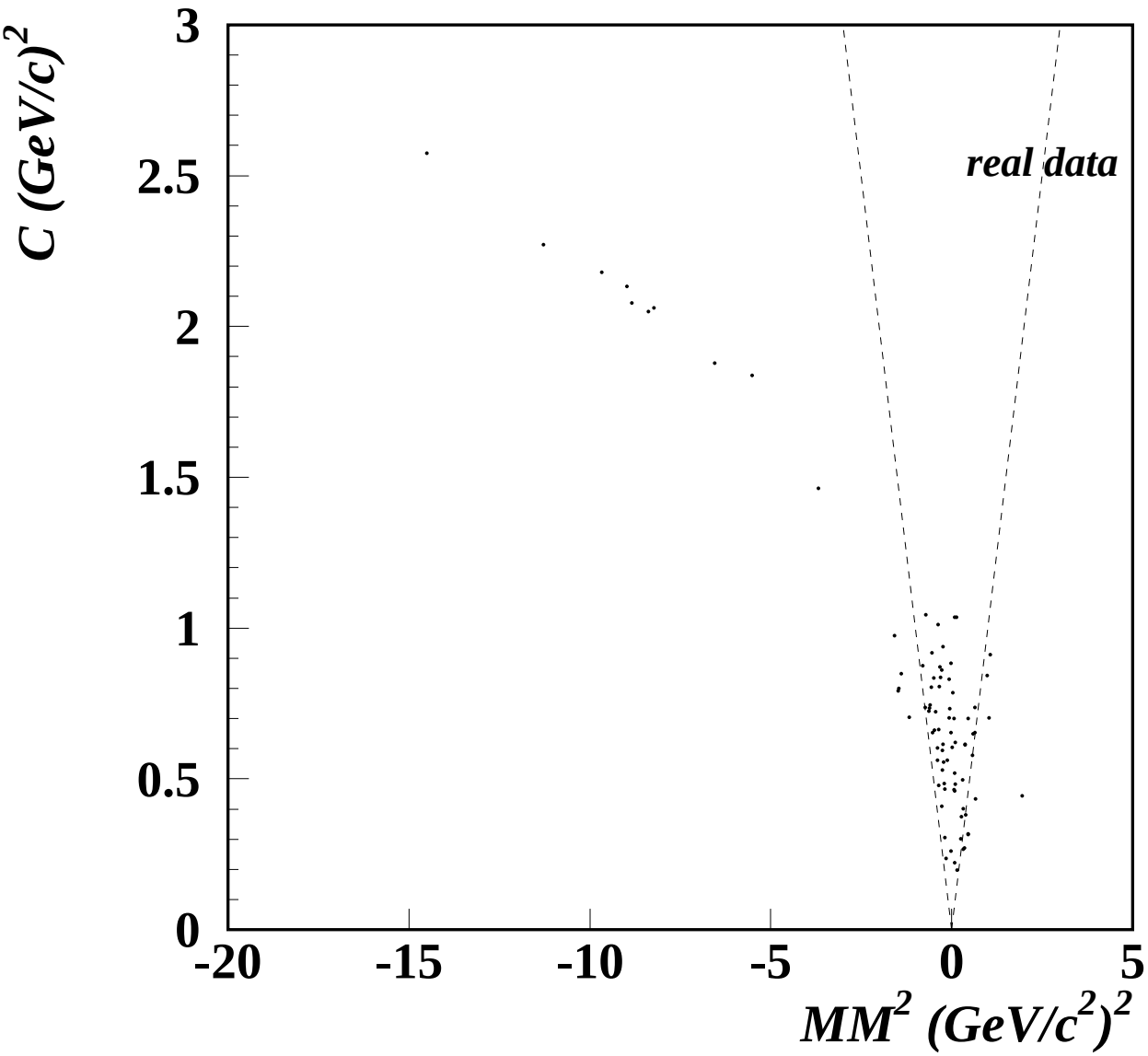

Figure 4.8: Distribution of C vs. MM^2 for real data events which pass all the cuts except for the C vs. MM^2 cut. The space between the dashed lines show the signal region.

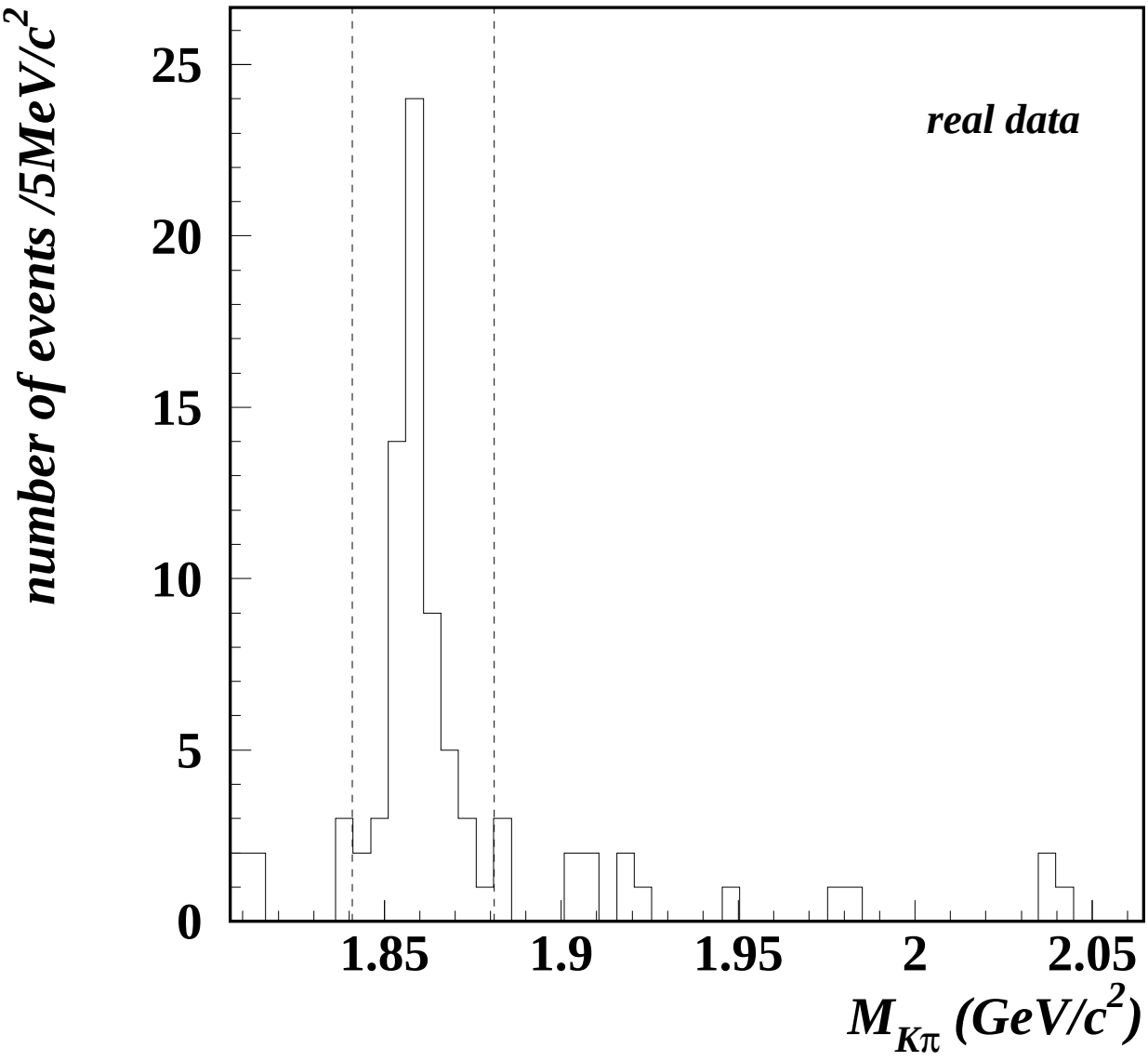

Figure 4.9: The $M_{K\pi}$ distribution of the events without flavor tagging after all the cuts except for that on $M_{K\pi}$. Dashed lines show the signal region.

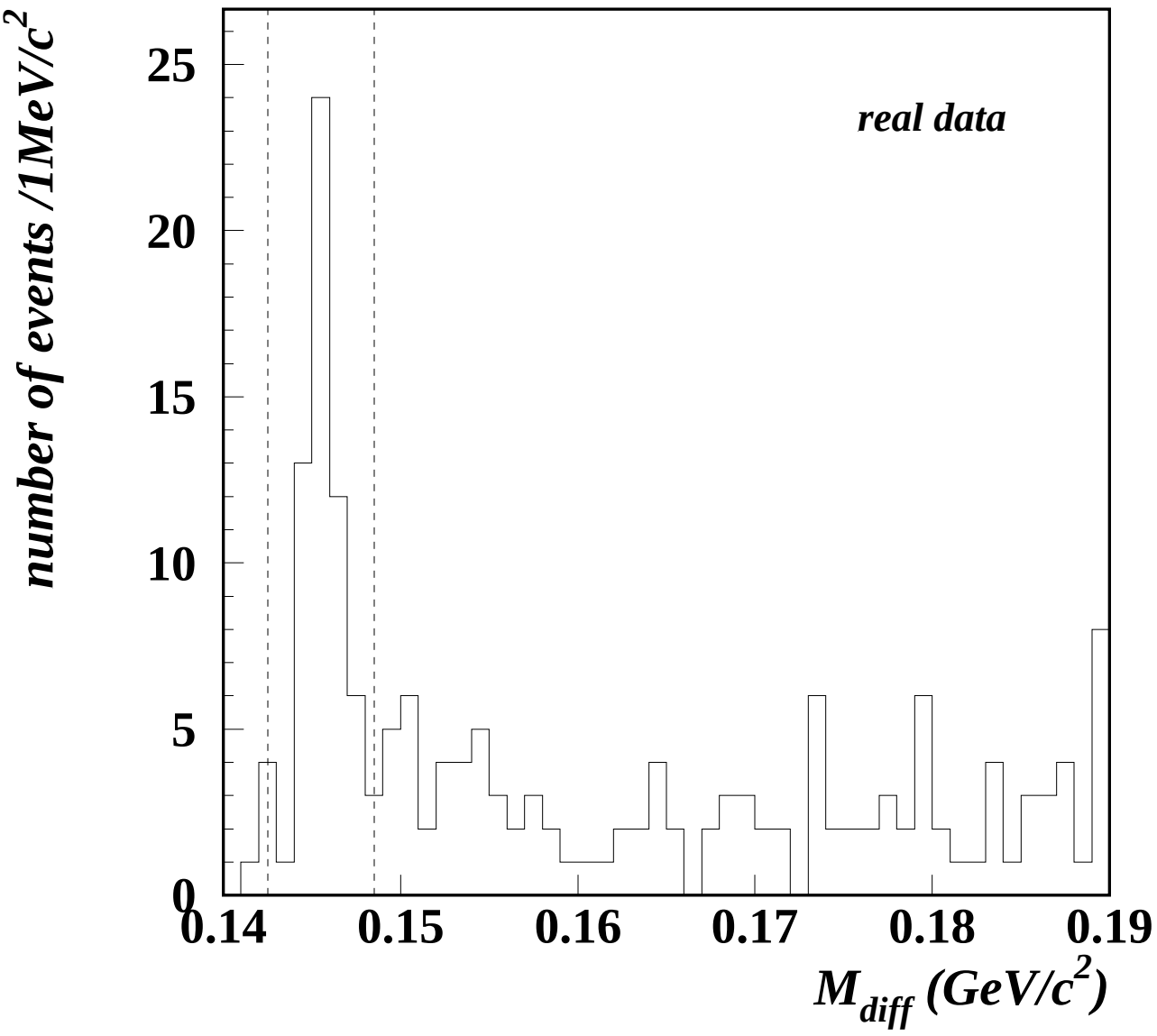

Figure 4.10: The M_{diff} distribution of the events without flavor tagging after all the cuts except for that on M_{diff}. Dashed lines show the signal region.

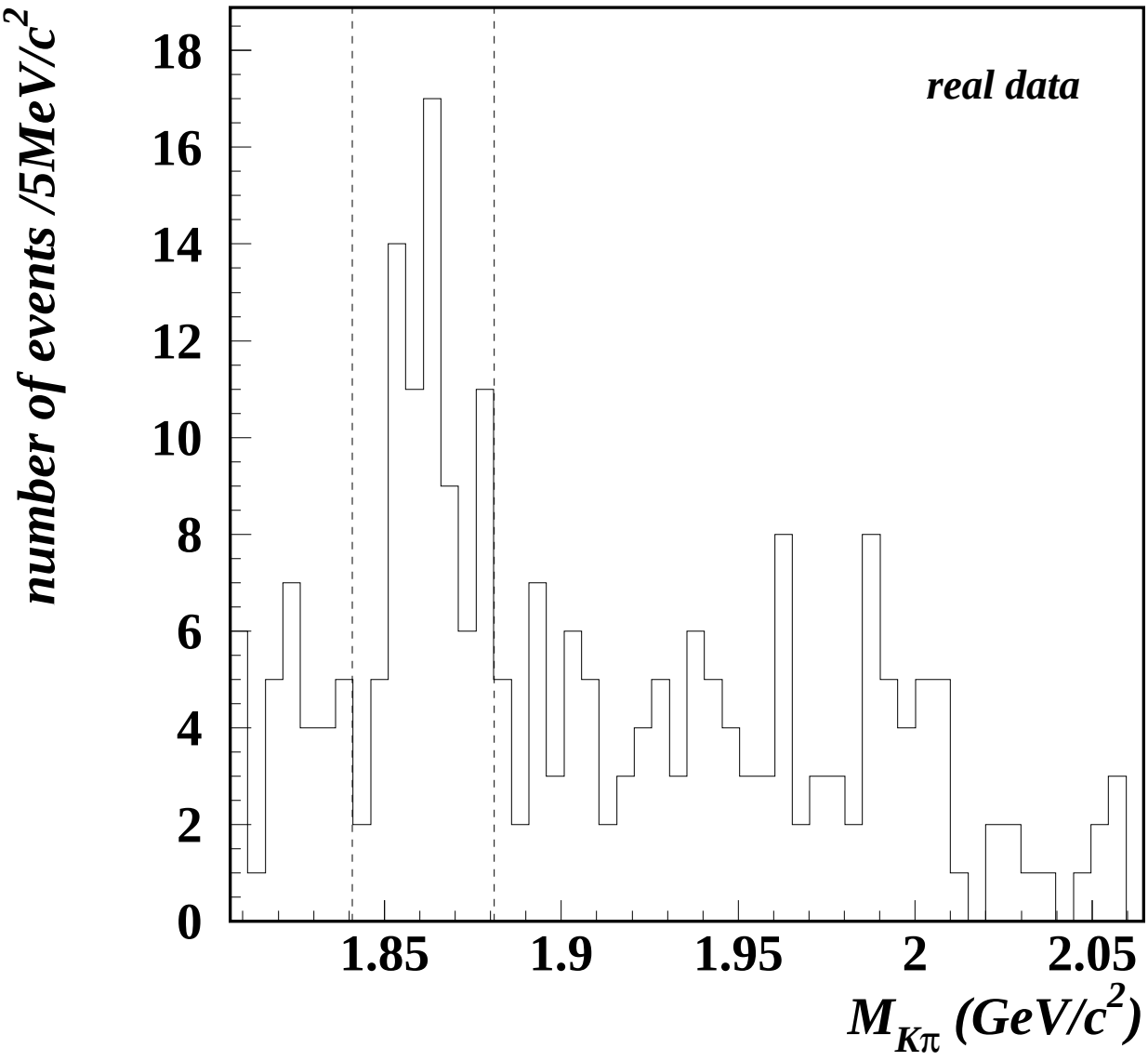

Figure 4.11: The $M_{K\pi}$ distribution of the events in the M_{diff} upper sideband region without flavor tagging after all the cuts except for that on $M_{K\pi}$. Dashed lines show the signal region.

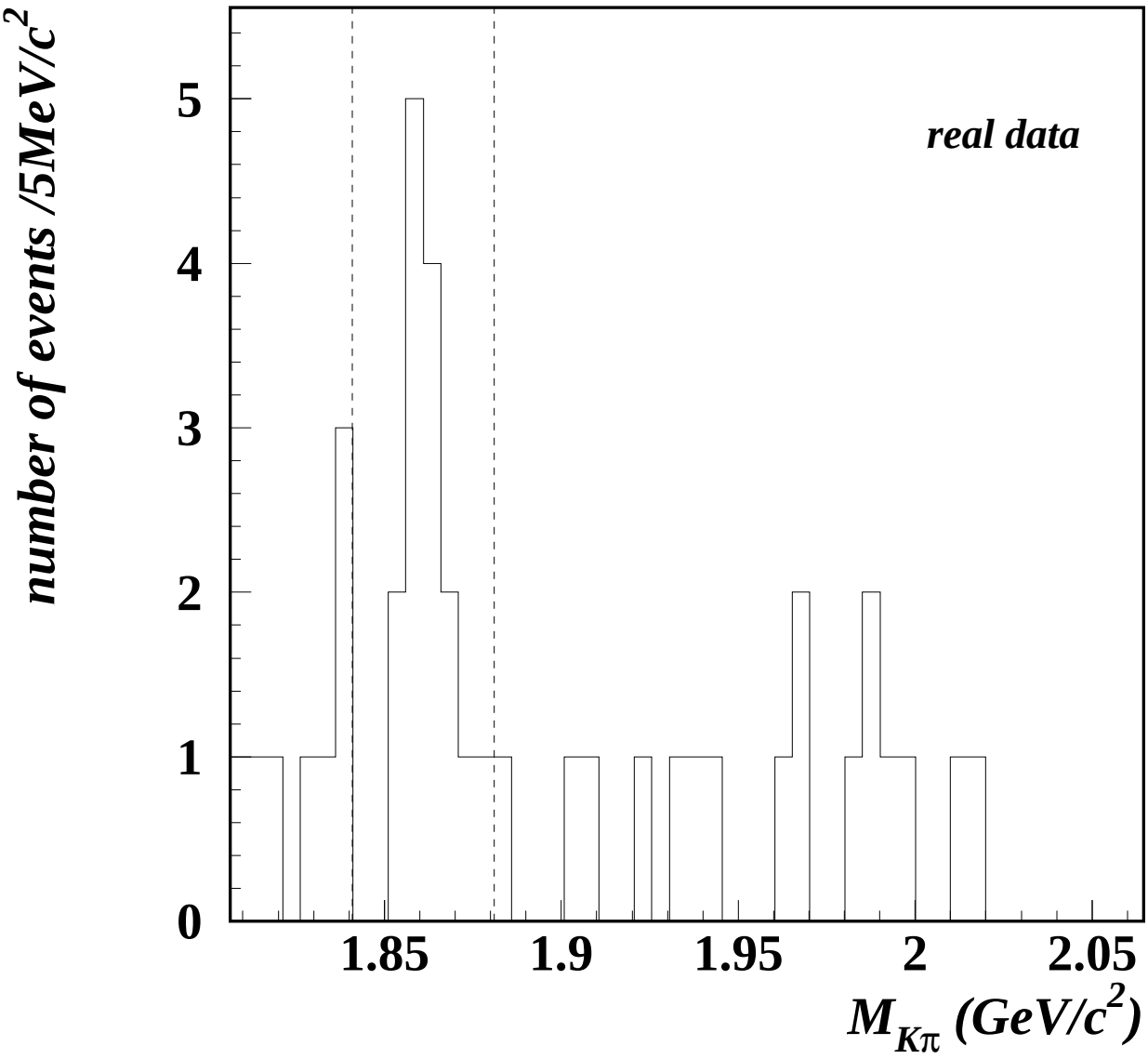

Figure 4.12: The $M_{K\pi}$ distribution of the events without flavor tagging in the $C < 0.8|MM^2|$ and $|MM^2| < 0$ region after application of all the cuts except for that on $M_{K\pi}$. Dashed lines show the signal region.

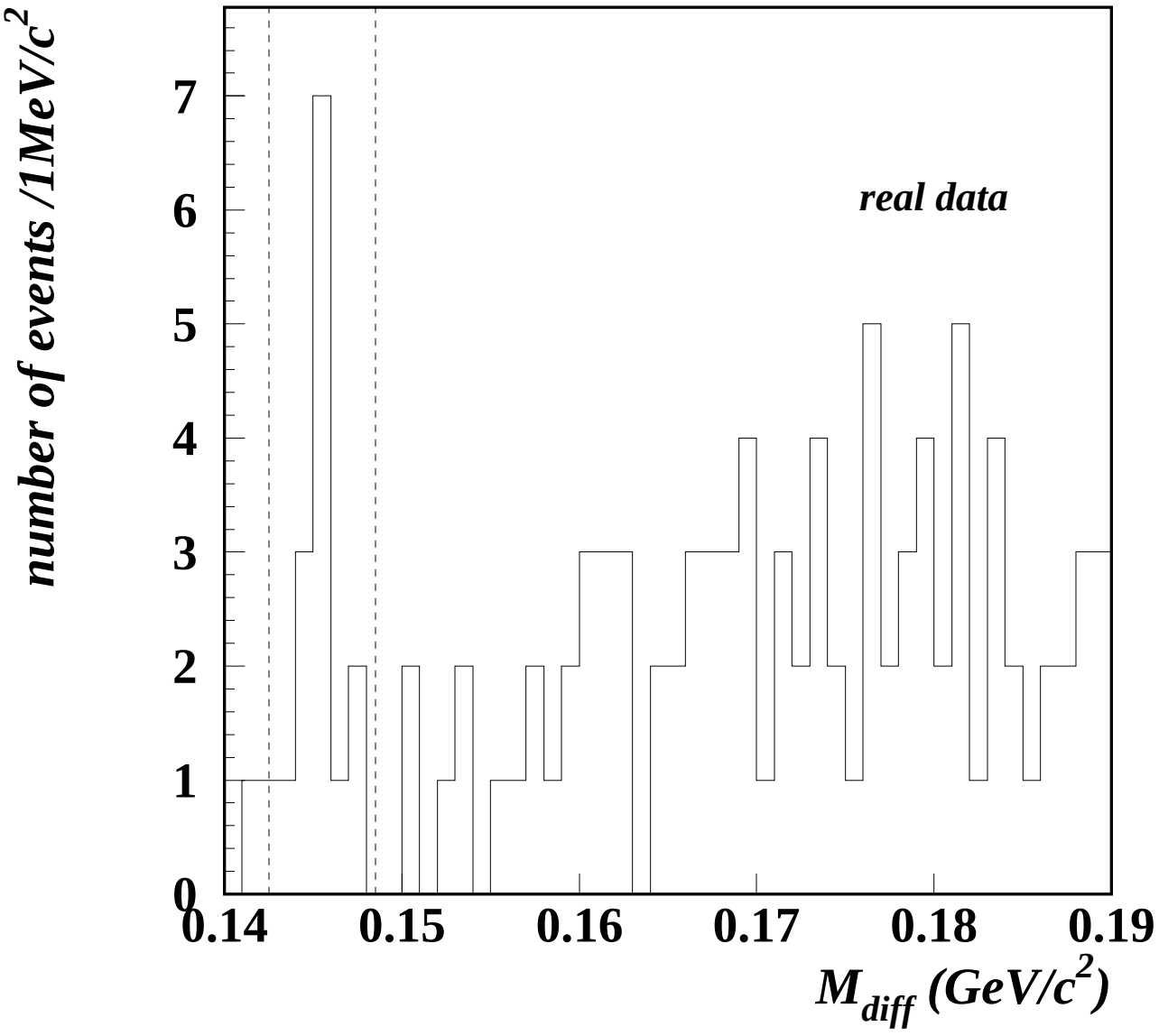

Figure 4.13: The M_{diff} distribution of the events without flavor tagging in the $C < 0.8|MM^2|$ and $|MM^2| < 0$ region after application of all the cuts except for that on M_{diff}. Dashed lines show the signal region.

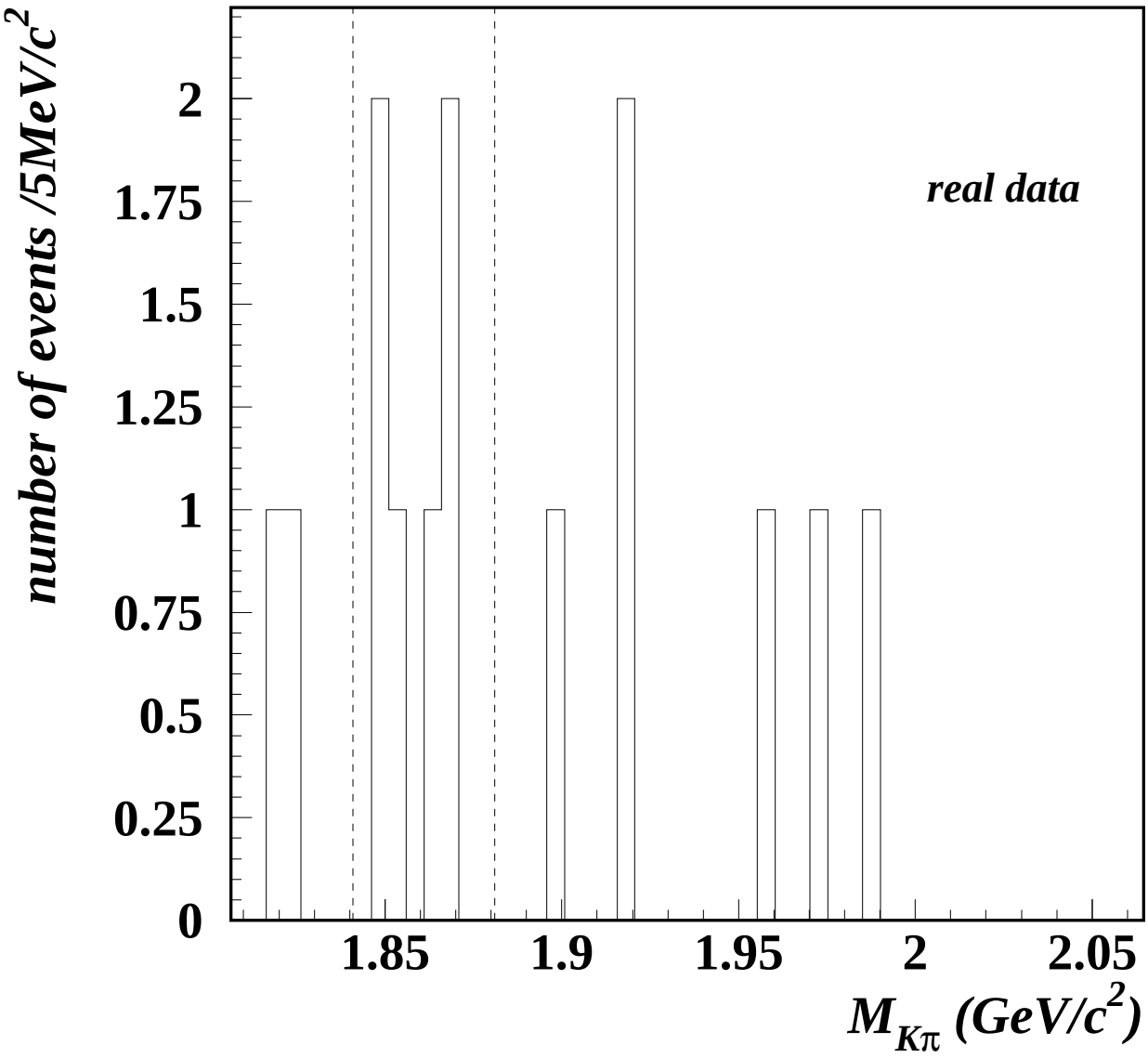

Figure 4.14: The $M_{K\pi}$ distribution of the events without flavor tagging in the $C < 0.8|MM^2|$ and $|MM^2| > 0$ region after application of all the cuts except for that on $M_{K\pi}$. Dashed lines show the signal region.

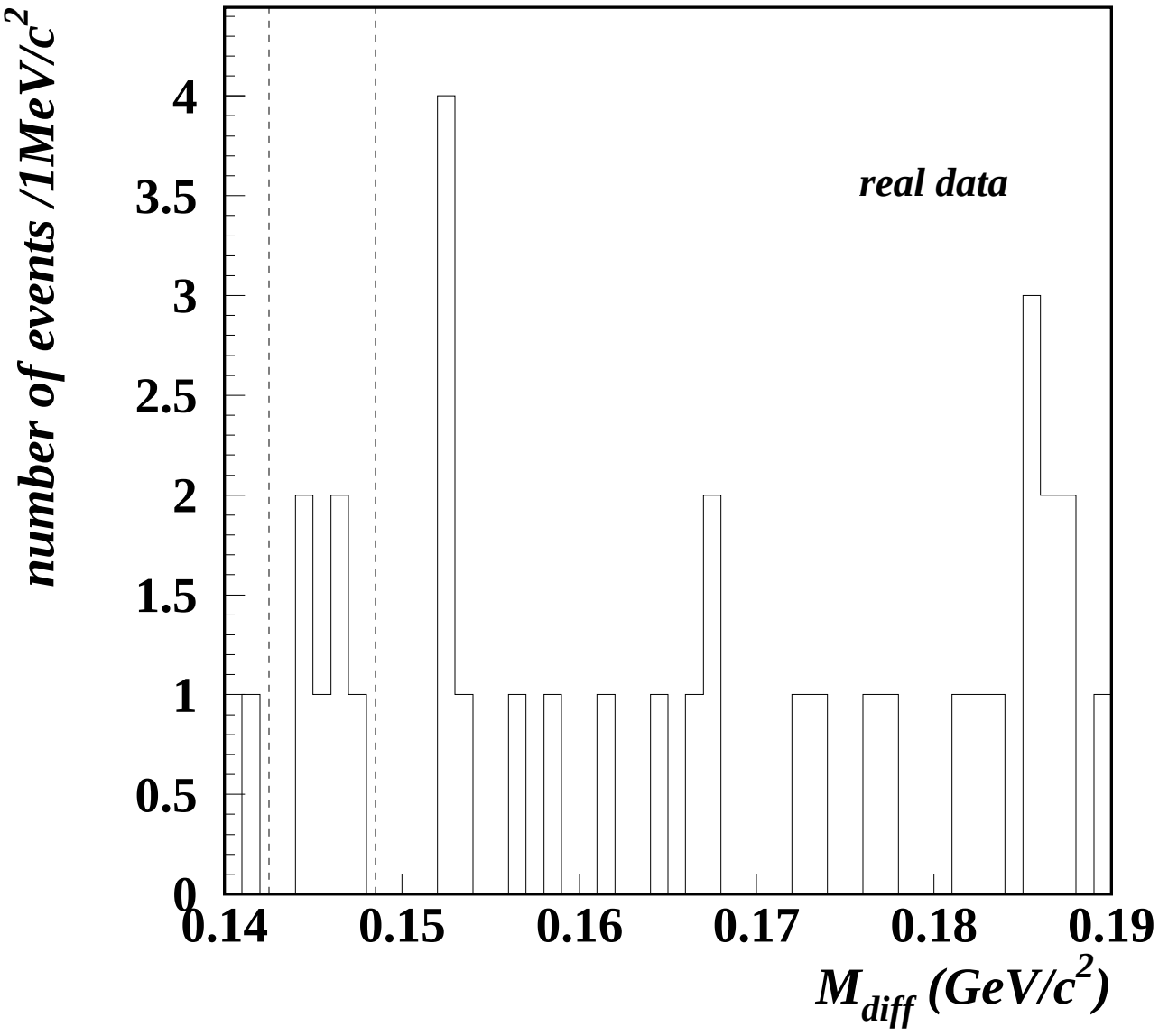

Figure 4.15: The M_{diff} distribution of the events without flavor tagging in the $C < 0.8|MM^2|$ and $|MM^2| > 0$ region after application of all the cuts except for that on M_{diff}. Dashed lines show the signal region.

Chapter 5

Conclusion

We studied flavor tagging of neutral B meson at the KEK B-factory. There are two requirements for flavor tagging. One is to maximize the effective efficiency (ϵ_{eff}), and the other is to estimate the wrong tagging fraction (ω) precisely.

To satisfy the former requirement, we performed a Monte Carlo study to maximize ϵ_{eff}. We found that by using the event missing momentum and the momentum of lepton simultaneously, we can use leptons with momentum in the center of mass system down to $0.6 GeV/c$ and raise ϵ_{eff} by about 1.0 % above that of the simple method with high momentum leptons and charge sum of kaons. We also studied the feasibility of using leptons from charm quarks and found that the wrong tagging fraction is large and contribution to ϵ_{eff} is only $0.215 \pm 0.009\%$. We obtained an effective efficiency of $25.05 \pm 0.07\%$ with leptons and kaons.

To estimate ω, we established the method to use $B^0(\overline{B}^0) \to D^{*\mp} l^{\pm} \nu$ decay in place of B_{cp}. From Monte Carlo study, for an integrated luminosity of 7fb^{-1}, we could estimate ω of flavor tagging with the simple method using leptons and kaons to be $11.0 \pm 2.9 \pm 1.0$, in which the first error is statistical and the second error is the uncertainty due to the mixing parameter. It is consistent with our Monte Carlo expectation and corresponds to an 8% error in the CP asymmetry which is smaller than the statistical error in the CP asymmetry for 100fb^{-1}, which is 12%. Therefore we conclude that this method can properly estimate ω and have enough accuracy for the CP violation measurement. We also tried to apply this method to the real data collected with the BELLE detector. We confirmed that the performance of flavor tagging on real data is consistent with the Monte Carlo expectation and the reconstruction of $B^0(\overline{B}^0) \to D^{*\mp} l^{\pm} \nu$ works properly.

Bibliography

[1] J. H. Christensen *et al.*, Phys. Rev. Lett. **13**, 138 (1964).

[2] M. Kobayashi and T. Maskawa, Prog. Theor. Phys. **49**, 652 (1973).

[3] I. I. Bigi and A. I. Sanda, "CP Violation", Cambridge University Press (1999).

[4] "KEKB B-Factory Design Report", KEK Report 95-7 (1995).

[5] BELLE Collaboration, "Technical Design Report", KEK Report 95-1 (1995).

[6] "CLEO software document home page":
http://www.lns.cornell.edu/public/CLEO/soft/QQ/index.html (1998).

[7] GEANT Detector Description and Simulation Tool, CERN Program Library Long Writeup W0513 (1993).

[8] Review of Particle Physics, C. Caso *et al*, The European Physics Journal, **3**, 1 (1998).

[9] G. C. Fox and S.Wolfram, Nucl. Phys. **B149**, 413 (1979).

[10] T. Kawasaki, PhD thesis, Osaka University, April 1999.

[11] The CLEO Collaboration, D. Besson *et al.*, Phys. Rev. Lett. **55**, 36 (1985)